

Light Water Reactor Sustainability Program

Risk-Informed Safety Margin Characterization Methods Development Work



September 2014

DOE Office of Nuclear Energy

DISCLAIMER

This information was prepared as an account of work sponsored by an agency of the U.S. Government. Neither the U.S. Government nor any agency thereof, nor any of their employees, makes any warranty, expressed or implied, or assumes any legal liability or responsibility for the accuracy, completeness, or usefulness, of any information, apparatus, product, or process disclosed, or represents that its use would not infringe privately owned rights. References herein to any specific commercial product, process, or service by trade name, trade mark, manufacturer, or otherwise, do not necessarily constitute or imply its endorsement, recommendation, or favoring by the U.S. Government or any agency thereof. The views and opinions of authors expressed herein do not necessarily state or reflect those of the U.S. Government or any agency thereof.

Light Water Reactor Sustainability Program

**Risk-Informed Safety Margin Characterization Methods
Development Work**

D. Mandelli, C. Smith, Z. Ma, T. Riley, J. Nielsen, A. Alfonsi, C. Rabiti, J. Cogliati

September 2014

**Idaho National Laboratory
Idaho Falls, Idaho 83415**

<http://www.inl.gov/lwrs>

**Prepared for the
U.S. Department of Energy
Office of Nuclear Energy
Under DOE Idaho Operations Office
Contract DE-AC07-05ID14517**

EXECUTIVE SUMMARY

This report summarizes the research activities realized during the Fiscal Year 2014 within the Risk Informed Safety Margin and Characterization (RISMC) pathway as part of the Light Water Reactor Sustainability (LWRS) Program. This research activity is complementary to the one presented in the INL/EXT-14-32906 report which shows advances in Probabilistic Risk Assessment (PRA) analysis using RAVEN and RELAP-7 in conjunction with novel flooding simulation tools.

Here we present several analyses that demonstrate the value of the RISMC approach in order to assess risk associated with nuclear power plants (NPPs). We focus on simulation based PRA which, in contrast to classical PRA, heavily employs system simulator codes. First, we compare, these two types of analyses, classical and RISMC, for a Boiling Water Reactor (BWR) Station Black Out (SBO) initiating event.

Second, we present an extended BWR SBO analysis using RAVEN and RELAP5-3D that addresses the comments and suggestions we received about the original analysis presented in INL/EXT-13-30203. This time we focus more on the stochastic analysis such probability of core damage and on the determination of the most risk-relevant factors.

Third, we show some preliminary results regarding the comparison between RELAP5-3D and the new code RELAP-7 using a simplified Pressurized Water Reactor system as a test case.

Lastly, we present some conceptual ideas regarding the possibility to extend the RISMC capabilities from an off-line tool (i.e., as PRA analysis tool) to an online-tool. In this new configuration, RISMC capabilities can be used to assist and inform the reactor operators during real accident scenarios as a decision-support tool.

CONTENTS

EXECUTIVE SUMMARY	ii
FIGURES	v
TABLES	vii
ACRONYMS	viii
1. Introduction	11
1.1 Structure of the report.....	12
2. RISMIC Simulation-Based Analysis Approach	13
2.1 The RISMIC toolkit.....	14
2.2 RAVEN framework.....	14
3. Improved BWR SBO Test Case	16
3.1 BWR model.....	16
3.2 SBO scenario.....	18
3.3 BWR model updates.....	21
3.3.1 RCIC and HPCI control logic	22
3.3.2 Battery logic.....	23
3.3.3 SRV activation logic	24
3.3.4 DG Logic.....	25
3.3.5 FW availability.....	26
3.4 Stochastic Parameters.....	27
3.5 Results	31
3.5.1 Stochastic analysis	32
3.5.2 Impact of auxiliary AC power systems (flex system).....	34
4. Classical PRA Compared to a Simulation-Based Approach	36
4.1 BWR simulated data.....	36
4.2 Classical PRA data	39
4.3 Comparison methodology	44
4.3.1 ET restructuring	45
4.3.2 Simulated data processing.....	47

4.4	Comparison results	48
5.	RELAP5-3D and RELAP-7 Initial Comparison	51
5.1	System description.....	51
5.2	Comparison results	54
5.2.1	Steady state results	54
5.2.2	Transient results	56
6.	RISMC Toolkit Enhancements.....	58
6.1	Diagnosis and prognosis: state of practice and state of the art.....	58
6.2	Merging data mining and machine learning.....	60
6.3	Basic machine learning.....	61
6.4	Temporal predictor	62
6.5	Data mining module	64
7.	Conclusions	67
	References.....	68
	Appendix A: Limit surface evaluation.....	71

FIGURES

Figure 1: Example of ET-FT structure for a BWR SBO initiating event	11
Figure 2: Structure of RAVEN statistical framework components	15
Figure 3: Overview of the BWR system with Mark I considered (a) and the AC/DC power system schematics (b).....	17
Figure 4: HCTL curves for PSP (top) and DW (bottom).....	18
Figure 5: Control logic scheme for the BWR system	20
Figure 6: RELAP5-3D nodalization of the BWR system	21
Figure 7: RCIC and HPCI control logic.....	22
Figure 8: RCIC control logic paired with DC system and SRV status: DC failure before (a) and after (b) ADS activation	23
Figure 9: Example of typical transient for DC system.....	23
Figure 10: DC control logic – example for three cases.....	24
Figure 11: SRV control logic paired with DC status for two different cases: DC failure before (a) and after (b) ADS activation.....	25
Figure 12: DG control logic paired with DC system for two cases: sampled battery failure time is before its lifetime (a) and after its lifetime (b).....	26
Figure 13: Plot of the pdfs of DG failure time (a) and DG recovery time (b)	28
Figure 14: Plot of the pdf of offsite power recovery.....	28
Figure 15: Plot of the pdfs of battery life (a) and clad failure temperature (b).....	29
Figure 16: Plot of the pdf of RCIC and HPCI failure time	29
Figure 17: Plot of the pdfs of firewater flow rate.....	30
Figure 18: Plot of the pdfs for battery recovery time (a) and firewater availability time (b).....	31
Figure 19: Simplified ET logic structure for a BWR SBO	32
Figure 20: Limit surface obtained in a two dimensional space (DG failure time vs. AC recovery time) for two different power level: 100% (left) and 120% (right).....	33
Figure 21: Plot of pdf for AC power recovery using FLEX system (to be compared with the pdf plotted in Figure 14)	34
Figure 22: BWR SBO simulated data: sequence/timing of events	37
Figure 23: ET structure for the BWR SBO model contained in SAPHIRE.....	39
Figure 24: ET structure for LOOP grid related; red path is characterized by the loss of DGs and leads to the SBO ET (see Figure 25)	40

Figure 25: ET structure for SBO.....	40
Figure 26: ET structure for one SRV stuck open.....	41
Figure 27: ET structure for two SRVs stuck open.....	42
Figure 28: Simplified SBO ET model.....	45
Figure 29: Output for each ET branch generated by the PYTHON script.....	48
Figure 30: Effect of DC system failure on max clad temperature histogram for scenarios leading to system OK.....	50
Figure 31: Scheme of the TMI PWR benchmark.....	51
Figure 32: Screenshot of the PWR model of RELAP-7 using PEACOCK.....	52
Figure 33: RELAP5-3D nodalization of the PWR model.....	53
Figure 34: Steady state analysis for the simplified PWR model using RELAP-7.....	54
Figure 35: Steady state analysis for the simplified PWR model using RELAP5-3D.....	55
Figure 36: Power transient considered.....	56
Figure 37: RELAP-7 transient results.....	57
Figure 38: RELAP5-3D transient results.....	57
Figure 39: Hypothetical ET structure for a LOOP initiating event.....	59
Figure 40: Core Damage probability (P_{CD}) value displayed by an hypothetical ET-FT based risk monitor (bottom) for a LOOP accident scenario (top) using the ET structure shown in Figure 39. The accident scenario is continuously matched with the ET structure. Such match for the accident scenario considered (top) is shown as a red line in Figure 39.....	59
Figure 41: RISMC diagnosis/prognosis framework.....	60
Figure 42: Example of 1-dimensional response surface.....	61
Figure 43: Example of a 2-dimensional response surface.....	62
Figure 44: Example of predicted temporal profile (left) given a set of simulated scenarios (right).....	64
Figure 45: Clustering of simulated scenarios into groups: representative scenarios [34].....	64
Figure 46: Symbolic conversion of time dependent data [39].....	65
Figure A-1: Limit surface evaluation using SVMs.....	71

TABLES

Table 1: Correspondence table between complexity and stress/stressor level and time values.....	30
Table 2: Summary of the stochastic parameters and their associated distributions	31
Table 3: Core damage probability for two different power levels (100% and 120%).....	32
Table 4: Branch probabilities associated to the ET shown in Figure 19 for both cases (100% and 120% power level).....	33
Table 5: Core damage probability for two different test cases (120% with and without FLEX system) ...	35
Table 6: Branch probabilities associated to the ET shown in Figure 19 for two different test cases (120% with and without FLEX system).....	35
Table 7: Correspondence table between complexity and stress/stressor level and time values.....	38
Table 8: List of stochastic parameters and their associated distribution.....	38
Table 9: SBO sequence quantification results for a typical BWR PRA model	43
Table 10: Simplified SBO model sequences versus original SBO model sequences	46
Table 11: Comparison of CD and OK probabilities.....	48
Table 12: Comparison of sequences (i.e., branch) probabilities (refer to the ET of Figure 28)	49
Table 13: Power distribution factor for representative channels and average pellet power.....	52
Table 14: Summary of the core channels average temperatures for RELAP5-3D and RELAP-7.....	55
Table 15: Computational time of search algorithm KNN for three different data set for both real-valued (original) and symbolic data.....	66

ACRONYMS

AC	Alternating Current
ADS	Automatic Depressurization System
BWR	Boiling Water Reactor
CDF	Cumulative Distribution Function
DC	Direct Current
DOE	Department of Energy
DG	Diesel generator
DW	Drywell
EOP	Emergency Operating Procedures
ET	Event-Tree
FT	Fault-Tree
FW	Firewater
GPM	Gaussian Process Model
GUI	Graphical User Interface
HPCI	High Pressure Core Injection
IE	Initiating Event
INL	Idaho National Laboratory
LOOP	Loss Of Offsite Power
LOOPGR	Loss Of Offsite Power Grid Related
LWR	Light Water Reactor
LWRS	Light Water Reactor Sustainability
MOOSE	Multi-physics Object-Oriented Simulation Environment
NPP	Nuclear Power Plant
PDF	Probability Distribution Function

PG	Power Grid
PRA	Probabilistic Risk Assessment
PSP	Pressure Suppression Pool
PWR	Pressurized Water Reactor
R&D	Research and Development
RCIC	Reactor Core Isolation Cooling
RISMC	Risk Informed Safety Margin Characterization
RPV	Reactor Pressure Vessel
SAMG	Severe Accident Management Guideline
SRV	Safety Relief Valve
T-H	Thermal-Hydraulics

Overview of the Risk-Informed Safety Margin Characterization Methods

1. INTRODUCTION

The scope of this report is to give an overview of the Research and Development (R&D) activities conducted in the Fiscal Year 2014 within the RISMC Pathway [1] in addition to the work reported in [2]. The RISMC Pathway aims to develop simulation-based tools and methods to assess risks for existing Nuclear Power Plants (NPPs) in order to optimize safety. This pathway, by developing new methods, is extending the state-of-the-practice methods which have been traditionally based on logic structures such as Event-Trees (ETs) and Fault-Trees (FTs) [3]. These static types of models mimic system response in an inductive and deductive way respectively, yet are restrictive in the ways they can represent spatial and temporal constructs.

An example of ET-FT structure is shown in Figure 1 for a simplified Station BlackOut (SBO) Initiating Event (IE). The ET structure shows how system success (i.e., outcome OK) can be achieved after a SBO accident scenario when either AC power is recovered or firewater (FW) is available. When neither of these two conditions is met, a core damage (CD) condition is reached. This logic progression is shown in the ET structure of Figure 1.

FTs are used to build logical event relationships between basic events (typically representing component failures) that affect branching conditions in the ET. In Figure 1, the two simplified FTs for AC and FW recovery are shown. For the first case, either Diesel Generators (DGs) or offsite Power Grid (PG) are sufficient conditions to recover AC power. In order to recover FW capabilities, the system needs to be depressurized (ADS) and FW outlet has to be aligned to the reactor vessel.

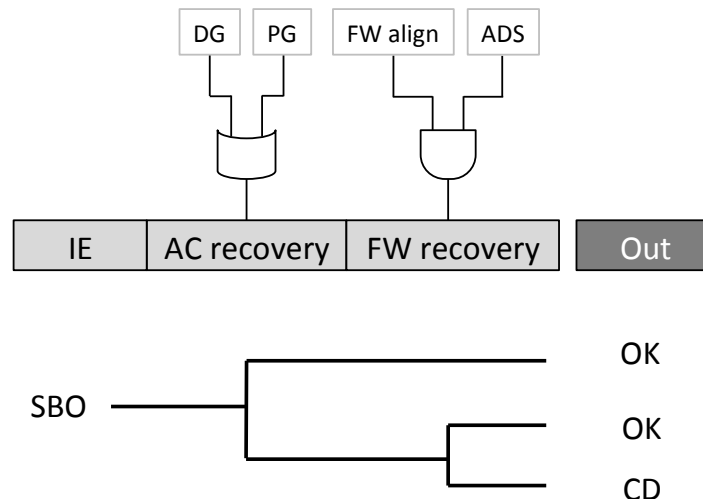


Figure 1: Example of ET-FT structure for a BWR SBO initiating event

Note that the structure shown in Figure 1 follows a precise logic that has been defined a priori by the user, i.e., the sequences of events in the ET are fixed and not interchangeable (in other words, they are part of a static model represented by a simple Boolean logic expression). As indicated in the historical accident in the nuclear industry, the timing of occurrence of such events can play a major role in the accident evolution. This timing information is not implicitly considered in an ET-FT structure shown in Figure 1; it is in fact only loosely considered in the definition of the basic events, e.g., DG recovery within 4 hours.

Both these issues (fixed logic structure, lack of timing considerations) preclude the ability to fully analyze possible accident evolution trajectories and, thus, also the possibility to evaluate importance of basic events in the overall CD probability. This is the reason why the RISMIC Pathway is employing state-of-the-art simulation based methodologies to evaluate accident evolution and the risk associated with these scenarios.

These issues are particularly relevant for the RISMIC project where it is needed to evaluate the impact of plant changes such as power uprates and life extension on existing NPPs. From an ET-FT logic point of view, both power uprate and life extensions are not modeled, which further shows the limitations of these kinds of methodologies for design and operational considerations.

In this report we describe the RISMIC approach and the RISMIC Toolkit [3]. We will show this approach applied to a BWR SBO test case and we will show how the results compare to the ones obtained using classical ET-FT methodologies. In addition we will show results regarding the possibility to extend RISMIC capabilities as an assisting tool for reactor operators during actual accident scenarios.

1.1 STRUCTURE OF THE REPORT

This report is structured as follows:

- **Section 2** – The RISMIC approach is described and the tools used are shown in detail: RAVEN, RELAP.
- **Section 3** – An extended BWR SBO analysis using RAVEN and RELAP5-3D is presented. This analysis focuses on the stochastic analysis performed to evaluate the increase of CD probability due to power uprate.
- **Section 4** – A comparison between the data generated using the RISMIC approach and the data generated through ET/FT based methodology using the SAPHIRE code is shown.
- **Section 5** – An initial comparison of RELAP5-3D and RELAP-7 for a simplified PWR test case is presented.
- **Section 6** – It is shown a conceptual extension of the RISMIC approach to cover diagnosis/prognosis capabilities to be employed as assisting tool for reactor operators during real accident scenarios.

2. RISM SIMULATION-BASED ANALYSIS APPROACH

In Section 1 we have shown the main reasons behind the choice of moving from an ET-FT logic structure and employing directly system simulator codes to perform PRA analyses. A simulator code is, per se, a tool that can be represented as:

$$\frac{\partial \boldsymbol{\theta}(t)}{\partial t} = \mathcal{H}(\boldsymbol{\theta}, \boldsymbol{p}, \boldsymbol{s}, t)$$

where:

- $\boldsymbol{\theta} = \boldsymbol{\theta}(t)$ represents the status of the system as function of time t , i.e., $\boldsymbol{\theta}(t)$ represents a single simulation
- \mathcal{H} is the actual simulator code that describes how $\boldsymbol{\theta}$ evolves in time
- \boldsymbol{p} is the set of parameters internal to the simulator code (e.g., pipe friction coefficients, pump flow rate, reactor power)
- $\boldsymbol{s} = \boldsymbol{s}(t)$ represents the status of components and systems of the simulator (e.g., status of emergency core cooling system, AC system)

By using the RISM approach, the PRA is performed by following these steps:

1. Associating a probabilistic distribution function (pdf) to the set of parameters \boldsymbol{p} and \boldsymbol{s} (e.g., timing of events)
2. Performing sampling of the pdfs defined in Step 1
3. Performing a simulation run given the \boldsymbol{p} and \boldsymbol{s} sampled in Step 2
4. Repeating Steps 2 and 3 N times and evaluate user defined stochastic parameters such CD probability (P_{CD}) as the ratio between the number of simulations that lead to CD divided by N (the total number of simulations).

Strictly speaking, the sampling associated to the vector of parameters \boldsymbol{p} is usually defined as uncertainty quantification while sampling the timing of events \boldsymbol{s} is usually called PRA. In our applications, we include in the definition of PRA the sampling of both \boldsymbol{p} and \boldsymbol{s} .

In order to perform PRA analyses of NPPs, the RISM Pathway has developed a toolkit which is described in detail in Section 2.1.

2.1 THE RISMC TOOLKIT

In order to perform advanced safety analysis, the RISMC Pathway has a toolkit that was developed internally at INL using MOOSE [2] as the underlying numerical solver framework. This toolkit consists of the following software tools:

- RELAP (both RELAP5-3D [4] and RELAP-7 [5]): the code responsible for simulating the thermal-hydraulic dynamics of the plant.
- RAVEN [6,7] (see Section 2.2): it has two main functions: 1) act as a controller of the RELAP-7 simulation and 2) generate multiple scenarios (i.e., a sampler) by stochastically changing the order and/or timing of events.
- PEACOCK: the Graphical User Interface (GUI) that allows the user to create/modify input files of both RAVEN and RELAP-7 [8] and to monitor the simulation in real time while it is running.
- GRIZZLY: the code that simulates the thermal-mechanical behavior of components in order to model component aging and degradation. Note that for the analysis described in this report, aging was not considered in the accident scenarios.

For the scope of this report, we mainly used RELAP and RAVEN to perform the PRA analyses.

2.2 RAVEN FRAMEWORK

The RAVEN statistical framework is a recent add-on of the RAVEN package that allows the user to perform generic statistical analysis. By statistical analysis we include:

- Sampling of codes: either stochastic (e.g., Monte-Carlo [9] and Latin Hypercube Sampling [10]) or deterministic (e.g., grid and Dynamic Event Tree [11])
- Generation of Reduced Order Models (ROMs) [12] also known as surrogate models or emulators
- Post-processing of the sampled data and generation of statistical parameters (e.g., mean, variance, covariance matrix)

Figure 2 shows an overview of the elements that comprise the RAVEN statistical framework:

- **Model:** it represents the pipeline between the input and output spaces. It is comprised of both mechanistic codes (e.g., RELAP-7) and ROMs
- **Sampler:** it is the driver for any specific sampling strategy (e.g., Monte-Carlo [13], Latin Hypercube Sampling [14], dynamic event trees [15])
- **Database:** the data storing entity
- **Post-processing:** module that perform statistical analyses and visualizes results

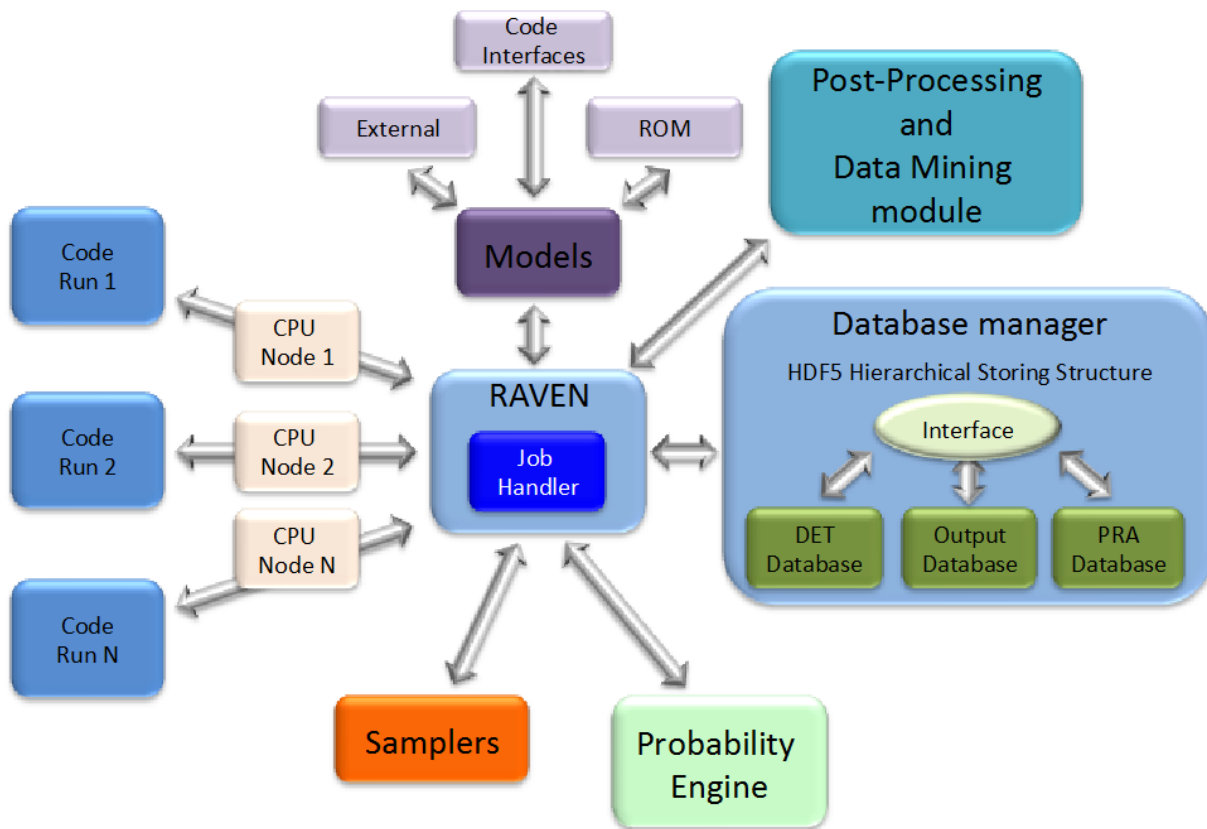


Figure 2: Structure of RAVEN statistical framework components

3. IMPROVED BWR SBO TEST CASE

This section shows the improved analysis performed for a BWR SBO test case using RELAP5-3D and RAVEN. The original analysis has been performed in [16] and the comments received on it suggested modifications in the system modeling part that would improve the validity of the analysis.

The modifications we performed were the following:

- Reactor Core Isolation Cooling System (RCIC) and High Pressure Coolant Injection (HPCI) control logic (see Section 3.3.1)
- Battery (i.e., DC power) control logic (see Section 3.3.2)
- Automatic Depressurization System (ADS) activation control logic (see Section 3.3.3)
- RCIC and HPCI control logic (see Section 3.3.4)
- DG control logic (see Section 3.3.5)
- FW system update (see Section 3.3.6)

Section 3.1 summarizes the BWR model that was originally implemented while Section 3.2 describes in more detail the model improvements listed above.

3.1 BWR MODEL

The system considered in this test case is a generic BWR power plant with a Mark I containment as shown in Figure 3. The three main structures are the following [16]:

- Reactor Pressure Vessel (RPV), it is the pressurized vessel that contains the reactor core.
- Primary containment includes:
 - Drywell (DW): it contains the RPV and circulation pumps
 - Pressure Suppression Pool (PSP) also known as wetwell: a large torus shaped container that contains a large amount of water; it is used as ultimate heat sink.
 - Reactor circulation pumps

While the original BWR Mark I includes a large number of systems, we consider a subset of it:

- RPV level control systems: provide manual/automatic control of the RPV water level:
 1. RCIC: Provide high-pressure injection of water from the CST to the RPV. Water flow is provided by a turbine driven pump that takes steam from the main steam line and discharges it to the suppression pool. Alternatively, the water source can be shifted from the CST to the PSP.
 2. HPCI: similar to RCIC, it allows greater water flow rates

- Safety Relief Valves (SRVs): DC powered valves that control and limit the RPV pressure.
- ADS: separate set of relief valves that are employed in order to depressurize the RPV.
- Cooling water inventory:
 1. Condensate Storage Tank (CST) that contains fresh water that can be used to cool the reactor core.
 2. PSP water: PSP contains a large amount of fresh water that is used to provide the ultimate heat sink when AC power is lost.
 3. Firewater system: water contained in the firewater system can be injected into the RPV when other water injection systems are disabled and when RPV is depressurized.

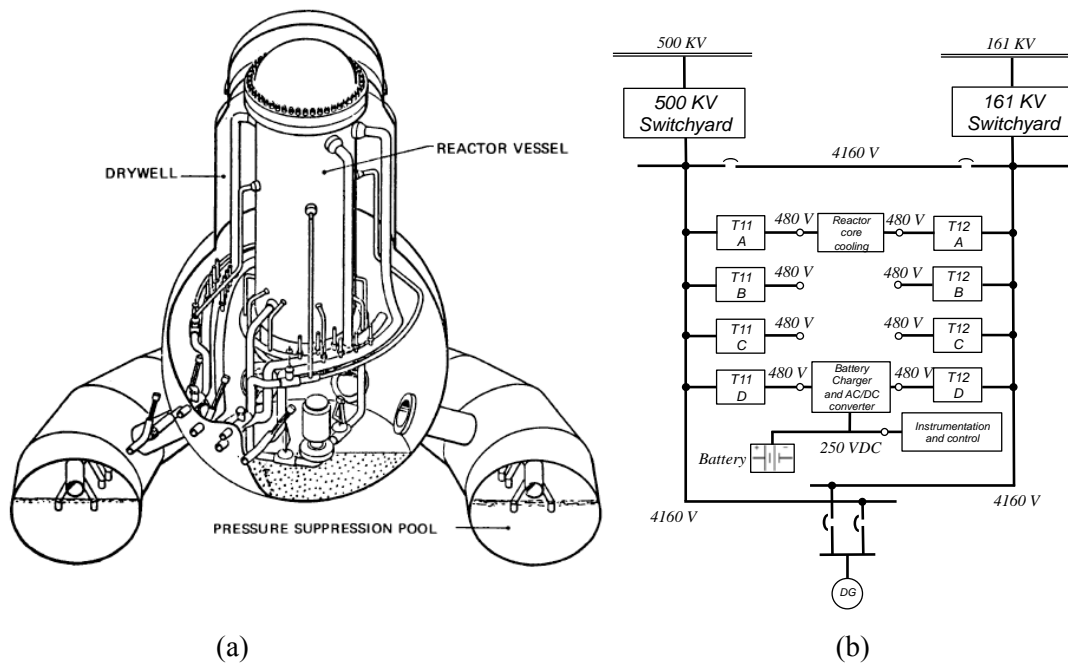


Figure 3: Overview of the BWR system with Mark I considered (a) and the AC/DC power system schematics (b)

- Power systems (see Figure 3 b):
 - Two independent power grids (500 KV and 161 KV) that are connected to the plant station through two independent switchyards. Loss of power from both switchyards disables the operability of all systems except: ADS, SRV, RCIC and HPCI (which requires only DC battery).
 - Diesel generators (DGs) which provide emergency AC power
 - Battery systems: instrumentation and control systems need DC power.

In an accident scenario, the set of emergency operating procedures requires the reactor operators to monitor not just the RPV but also the containment (both DW and PSP) thermo-hydraulic parameters (level, pressure and temperature). In particular, a set of limit curves is provided so that when they are crossed, the operators are required to activate the ADS system. These limit curves, also known as Heat Capacity Temperature Limits (HCTL), are shown in Figure 4 for both PSP and DW.

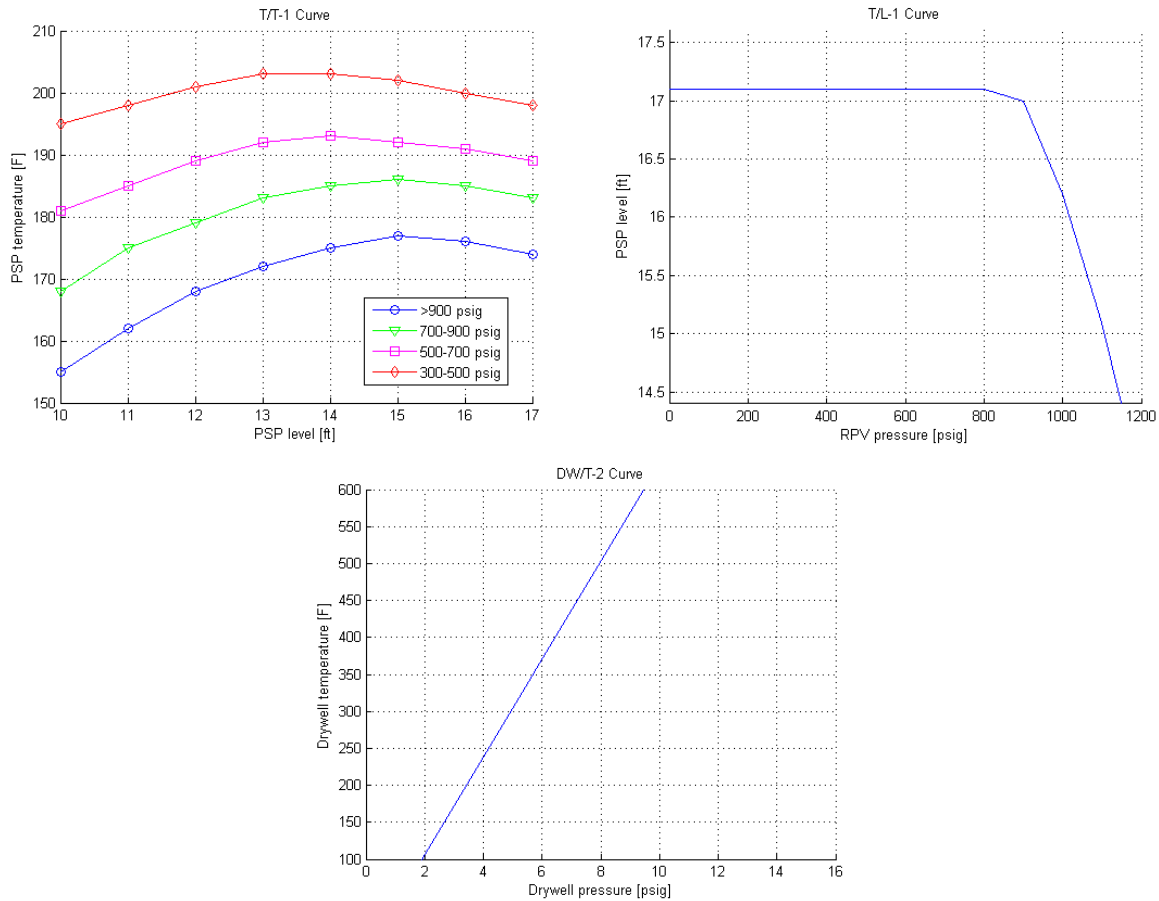


Figure 4: HCTL curves for PSP (top) and DW (bottom)

3.2 SBO SCENARIO

The accident scenario under consideration is a loss of off-site power (LOOP) followed by loss of the DGs, i.e. SBO initiating event. In more detail (Figure 5):

- At time $t = 0$: the following events occur:
 - LOOP condition occurs due to external events (i.e., power grid related)
 - LOOP alarm triggers the following actions:
 - Operators successfully scram the reactor and put it in sub-critical conditions by fully inserting the control rods in the core

- Emergency DGs successfully start, i.e., AC power is available
- Core decay heat is removed from the RPV through the RHR system
- DC systems (i.e., batteries) are functional
- SBO condition occurs: due to internal failure, the set of DGs fails, thus removal of decay heat is impeded. Reactor operators start the SBO emergency operating procedures and perform:
 - RPV level control using RCIC or HPCI
 - RPV pressure control using SRVs
 - Containment monitoring (both drywell and PSP)
- Plant operators start recovery operations to bring back on-line the DGs while the recovery of the power grid is underway by the grid owner emergency staff
- Due to the limited life of the battery system and depending on the use of DC power, battery power can deplete. When this happens, all remaining control systems are offline causing the reactor core to heat until clad failure temperature is reached, i.e., core damage (CD)
- If DC power is still available and one of these conditions are reached:
 - Failure of both RCIC and HPCI
 - HCTL limits reached
 - Low RPV water level

then the reactor operators activate the ADS system in order to depressurize the RPV

- Firewater injection: as an emergency action, when RPV pressure is below 100 psi plant staff can connect the firewater system to the RPV in order to cool the core and maintain an adequate water level. Such task is, however, hard to complete since physical connection between the firewater system and the RPV inlet has to be made manually
- When AC power is recovered, through successful re-start/repair of DGs or off-site power, RHR can be now employed to keep the reactor core cool.

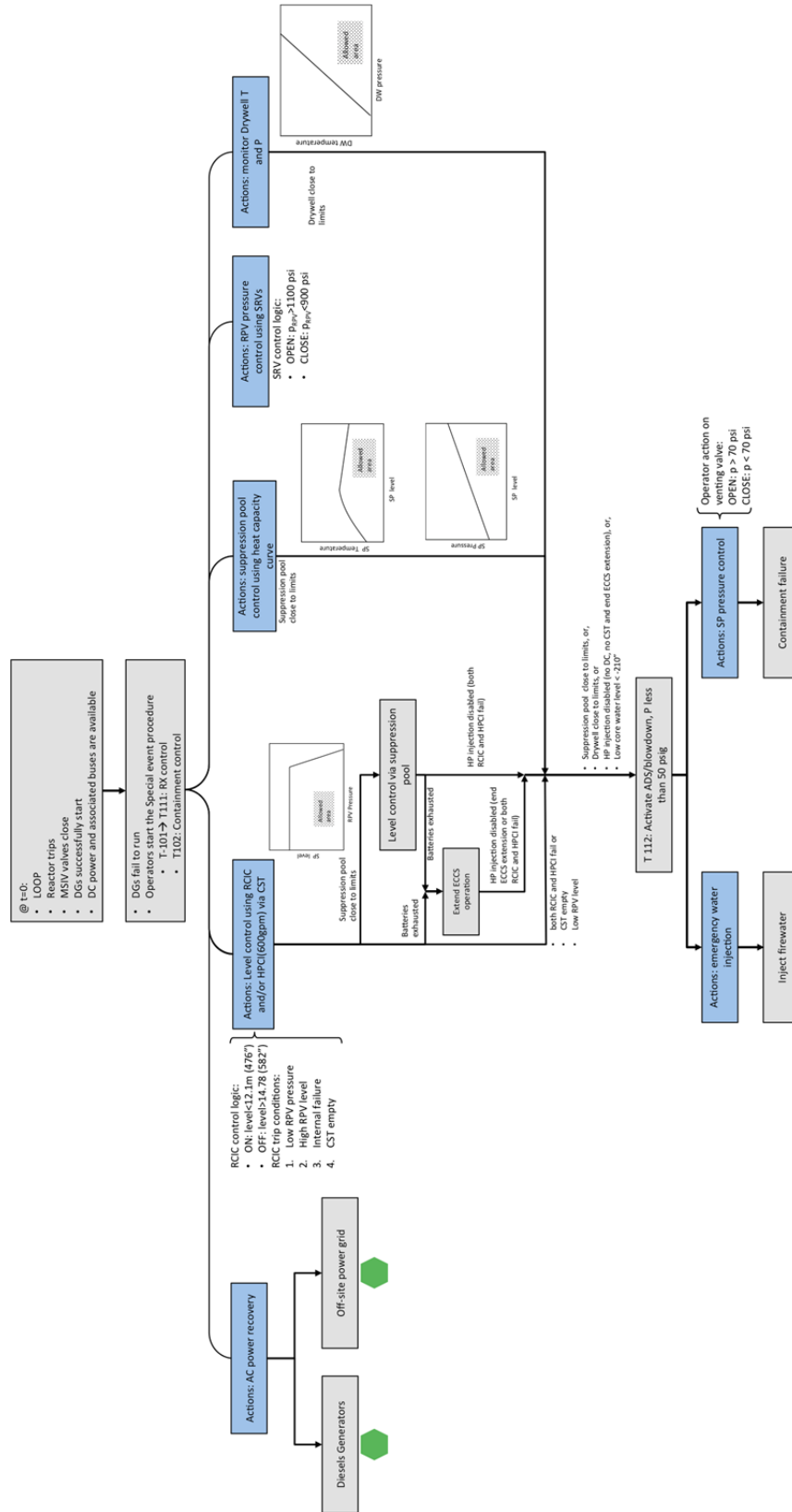


Figure 5: Control logic scheme for the BWR system

3.3.1 RCIC AND HPCI CONTROL LOGIC

The HPCI and RCIC logic update was the most extensive of the revisions. In the original system [16], HPCI and RCIC would simply turn off when the DC power failed, and there was no possibility for DC recovery or for turbine flooding.

The logic was updated to reflect the possibility of the valves controlling the HPCI/RCIC turbine becoming stuck open when battery power was lost, rather than the prior, incorrect assumption that they would fail closed. Additionally, when the valve is stuck open and HPCI/RCIC is stuck in an ‘ON’ configuration, it was possible that the core would become overfilled and the main steam line would flood, permanently disabling HPCI/RCIC for the rest of the transient, and possibly irreparably damaging the HPCI/RCIC turbine. A map of the operational states of HPCI/RCIC and the pathways between these states is shown Figure 7.

The pathways between these operational states reflect that it is possible for HPCI and/or RCIC to fail at any given point during normal operations, or when the HPCI/RCIC turbine is stuck open or closed. For the turbine to become stuck open, battery power must fail while it is already open and HPCI/RCIC is running, and for the turbine to become stuck closed, battery power must fail while it is already closed and HPCI/RCIC is not running. If the turbine becomes stuck open, it is possible that, before battery power can be recovered and the turbine shut when appropriate, HPCI and/or RCIC will overfill the core and flood the HPCI/RCIC turbine, permanently disabling the system. This is shown in the pathway from “Stuck Open” to “Failed” labeled “Failure or flood.” An example of HPCI/RCIC control logic scenario is shown in Figure 9.

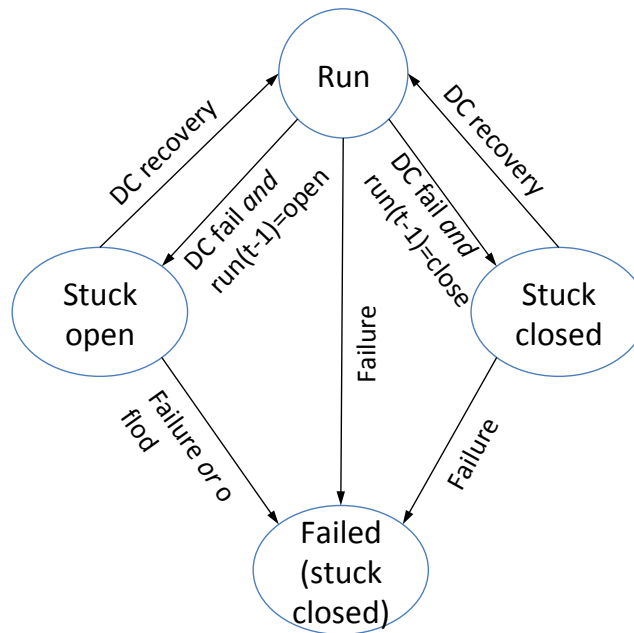


Figure 7: RCIC and HPCI control logic

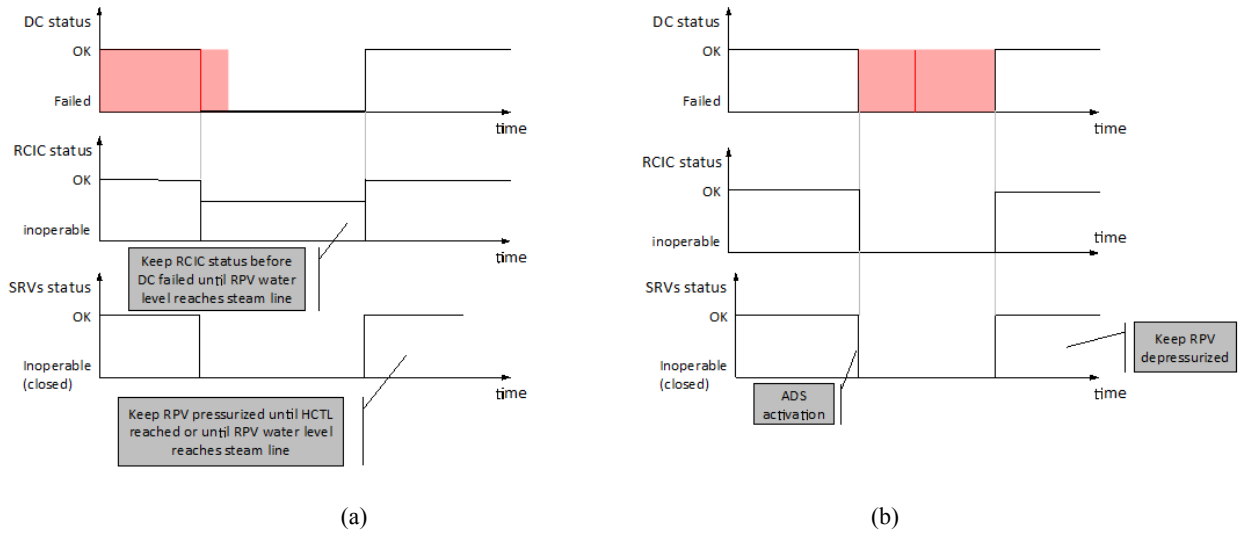


Figure 8: RCIC control logic paired with DC system and SRV status: DC failure before (a) and after (b) ADS activation

3.3.2 BATTERY LOGIC

In the original system, DC power from batteries simply had a randomly sampled lifetime, and when it failed, was permanently disabled. Under the new approach, the DC power can fail due to the batteries running out or to 'external failure (failure other than running out of stored power), with these two different kinds of failure affecting the model in different ways. Additionally, there is a randomly sampled 'repair time' for the DC power, during which the operators prepare and connect an alternate source of DC power, such as a portable DC generator. This is displayed visually in Figure 9 and Figure 10.

If the batteries run out of power or fail, the DC power recovery process begins immediately and is resolved after a randomly sampled time (battery recovery time, which could include a delay period if needed). Should the timing of the battery power failure occur after the batteries have run out, but before an alternate DC power source can be implemented, it has no effect – the batteries are dead, and the fact that they are now both dead and broken does not matter. Likewise, if the batteries fail after alternate DC power has been implemented, it again does not matter than the batteries are both dead and broken instead of simply dead. After DC power has been recovered, if the HPCI/RCIC turbine did not flood during the DC power failure, those systems resume normal operations if they have not failed on demand.

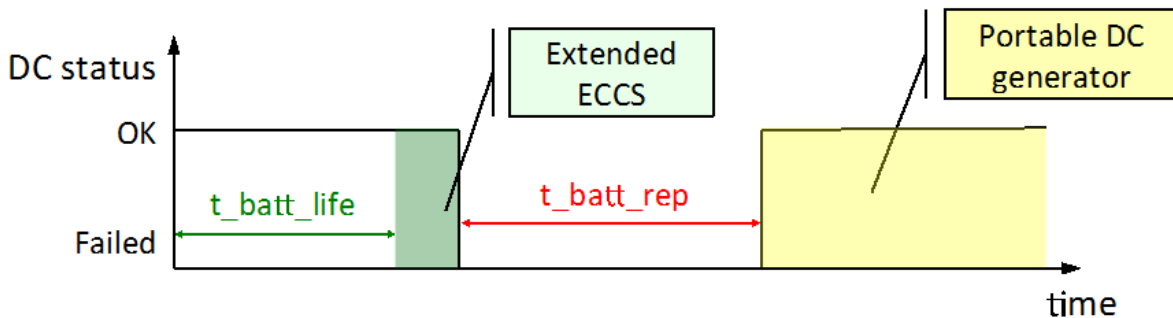


Figure 9: Example of typical transient for DC system

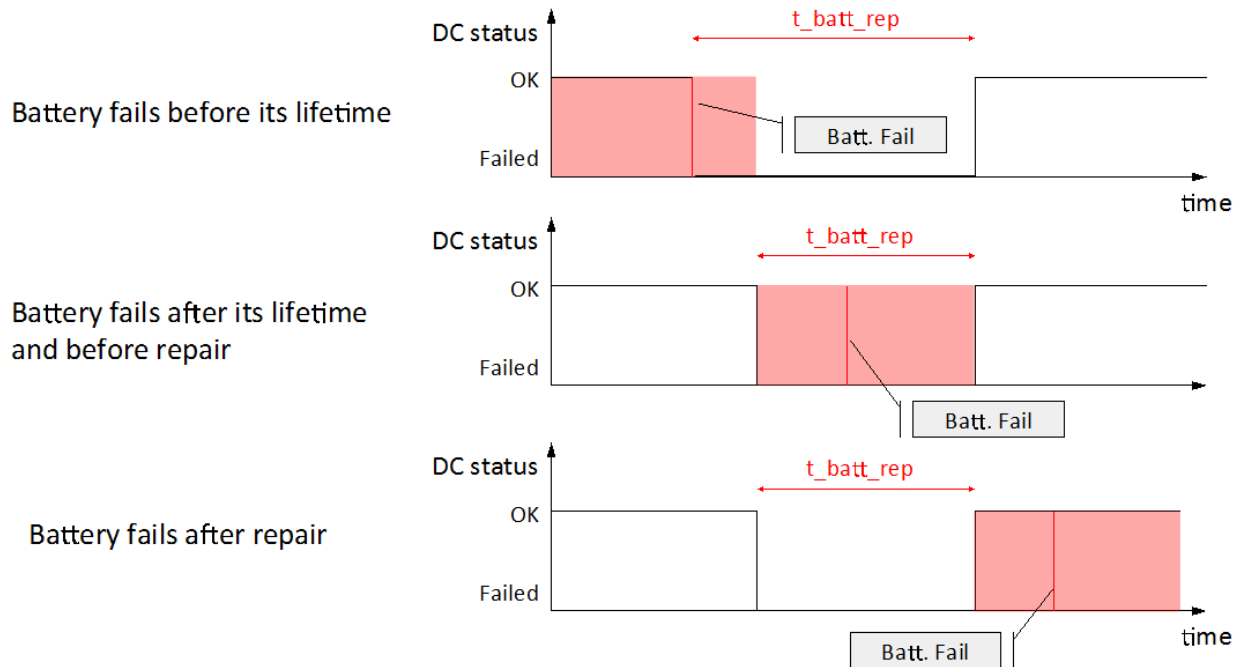


Figure 10: DC control logic – example for three cases

3.3.3 SRV ACTIVATION LOGIC

The SRV activation logic modification was a straightforward update. It was expected that the plant operators would be able to predict when the DC power supply from emergency batteries was close to the end of its operational lifetime (the batteries are running out) and would activate the ADS preemptively to better allow for firewater alignment, forestalling the potential for core damage. Accordingly, ten minutes before the end of battery lifetime, the ADS is activated and RPV pressure drops. However, if the DC power fails because the batteries fail, i.e. they still have power left but are non-functional due to some unforeseen equipment failure, the operators will have no foreknowledge of this event and the DC power will fail without the ADS activating, and the SRVs will fail shut and prevent ADS activation.

When DC power is recovered, if the ADS was previously activated and the RPV depressurized before DC power was lost, then the SRVs will be used to keep the RPV depressurized and the operators rely on firewater to keep the core cooled. Otherwise, if the RPV was not depressurized before ADS activation, the operators will keep the RPV pressurized until the wetwell heat limits are reached, at which point they will activate the ADS, depressurize the RPV, and switch to firewater. This modeled behavior is displayed in Figure 11.

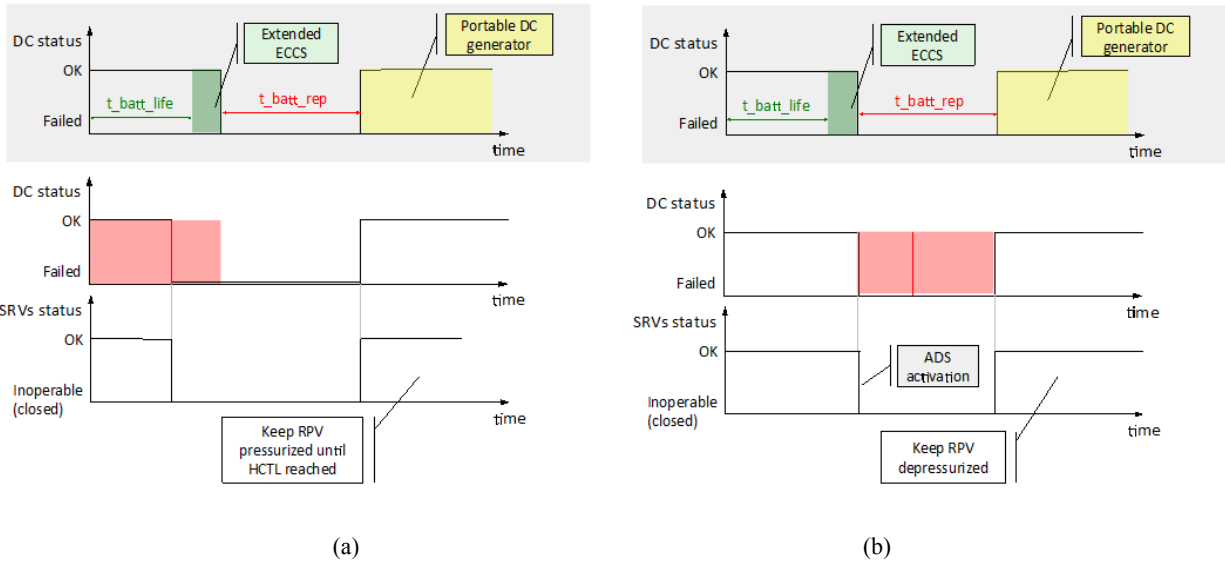


Figure 11: SRV control logic paired with DC status for two different cases: DC failure before (a) and after (b) ADS activation

3.3.4 DG LOGIC

The modification of the DG logic was also a straightforward update. Previously, an assumption was made that the DGs would be recoverable without having DC power to start them up. This was changed, and the DGs can no longer be recovered (which would end the simulation in success) unless DC power is operational. If the DGs are ready to be turned on when DC power is recovered, the simulation will end in success (see Figure 12). Offsite power recovery was not changed, and can be recovered without DC power. Recovering either source of AC site power will immediately end the simulation in success.

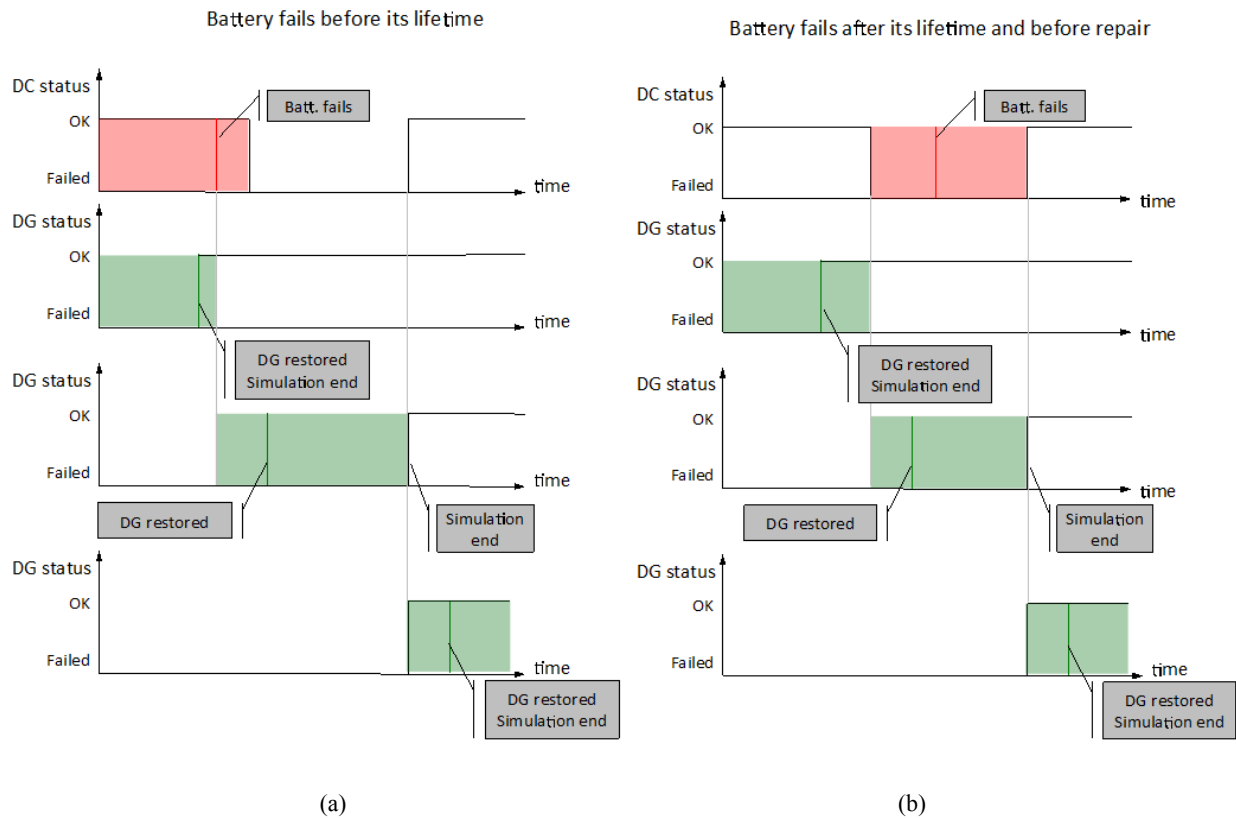


Figure 12: DG control logic paired with DC system for two cases: sampled battery failure time is before its lifetime (a) and after its lifetime (b)

3.3.5 FW AVAILABILITY

Previously, when FW alignment was completed and the RPV depressurized to the point that firewater injection could begin, the simulation ended immediately in success. This was unrealistic, and was changed. Under the updated firewater injection, once the firewater is aligned and the RPV depressurized, water is injected into the core at a randomly sampled mass flow rate for as long as core pressure remains below the operational pressure threshold of the firewater. This refloods the core if the firewater injection is of sufficient mass flow rate to cool the core, in an attempt to prolong core damage long enough for AC power to be recovered.

3.4 STOCHASTIC PARAMETERS

For this analysis we considered several uncertain parameters:

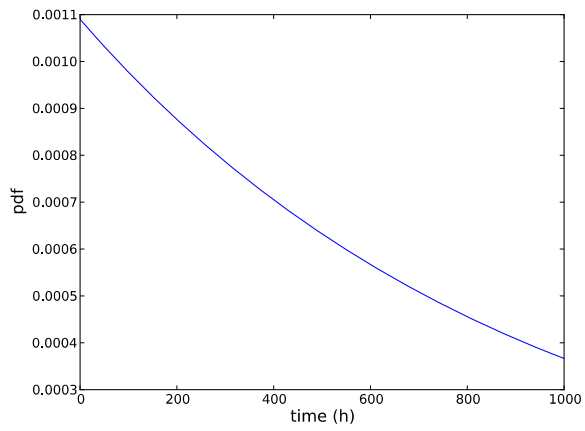
- **Failure time of DGs:** regarding the time at which the DGs fail to run we chose an exponential distribution with a value of lambda equal to $1.09 \cdot 10^{-3} \text{ h}^{-1}$ as indicated by NRC published data [18] (see Figure 13 a).
- **Recovery time of DGs:** Regarding time needed to recover the DGs, we used as a reference the NUREG/CR-6890 vol.1 [17]. This document uses a Weibull distribution¹ with $\alpha = 0.745$ and $\beta = 6.14 \text{ h}$ (mean = 7.4 h and median = 3.8 h). Such distribution (see Figure 13 b) represents the pdf of repair of one of the two DGs (choosing the one easiest to repair).
- **Offsite AC power recovery:** For the time needed to recover the off-site power grid, we used as reference NUREG/CR-6890 vol.2 [18] (data collection was performed between 1986 and 2004). Given the four possible LOOP categories (plant centered, switchyard centered, grid related or weather related), severe/extreme events (such as earthquake) are assumed to be similar to these events found in the weather category (these are typically long-term types of recoveries). This category is represented with a lognormal distribution (from NUREG/CR-6890 [18]) with $\mu = 0.793$ and $\sigma = 1.982$ (see Figure 14).
- **Battery life:** For the amount of DC power available, when AC power is not obtainable, we chose to limit battery life between 4 and 6 hours using a triangular distribution (see NUREG/CR-6890 vol.2 as reference [18]) as shown in Figure 15 a.
- **Battery failure time:** As basic event in the PRA model, the probability value associated with battery failure is equal to $1.4 \cdot 10^{-5}$ for an expected life of 4 hours. We have assumed an exponential distribution for the battery failure time distribution. The value of λ for this distribution has been calculated by imposing that the CDF of this distribution ($1 - e^{-\lambda t}$) at 4 hours (i.e., the probability that battery fails within 4 hours is $1.4 \cdot 10^{-5}$):

$$\int_0^4 \lambda e^{-\lambda t} dt = [1 - e^{-\lambda t}]_0^4 = 1.4 \cdot 10^{-5}$$

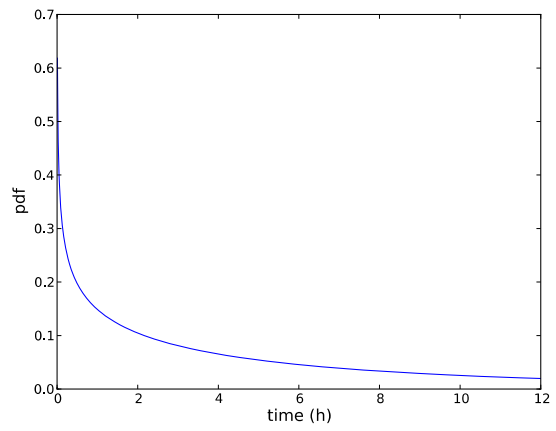
This leads to a value of $\lambda = 3.5 \cdot 10^{-6}/\text{hr}$.

- **SRVs fails open time:** the SPAR model indicates a probability value of $8.56 \cdot 10^{-4}$.
- **Clad Fail temperature:** Uncertainty in failure temperature for the clad is characterized by a triangular distribution [19] having (see Figure 15 b):
 - Lower limit = 1800 F (982 C): PRA success criterion
 - Upper limit = 2600 F (1427 C): Urbanic-Heidrick transition temperature
 - Mode = 2200 F (1204 C): 10 CFR regulatory limit

¹ Weibull distribution $pdf(x)$ is here defined as: $pdf(x) = \frac{\alpha}{\beta^\alpha} x^{\alpha-1} e^{-\left(\frac{x}{\beta}\right)^\alpha}$



(a)



(b)

Figure 13: Plot of the pdfs of DG failure time (a) and DG recovery time (b)

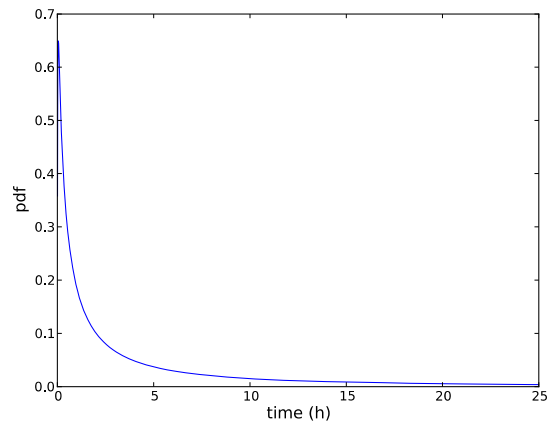


Figure 14: Plot of the pdf of offsite power recovery

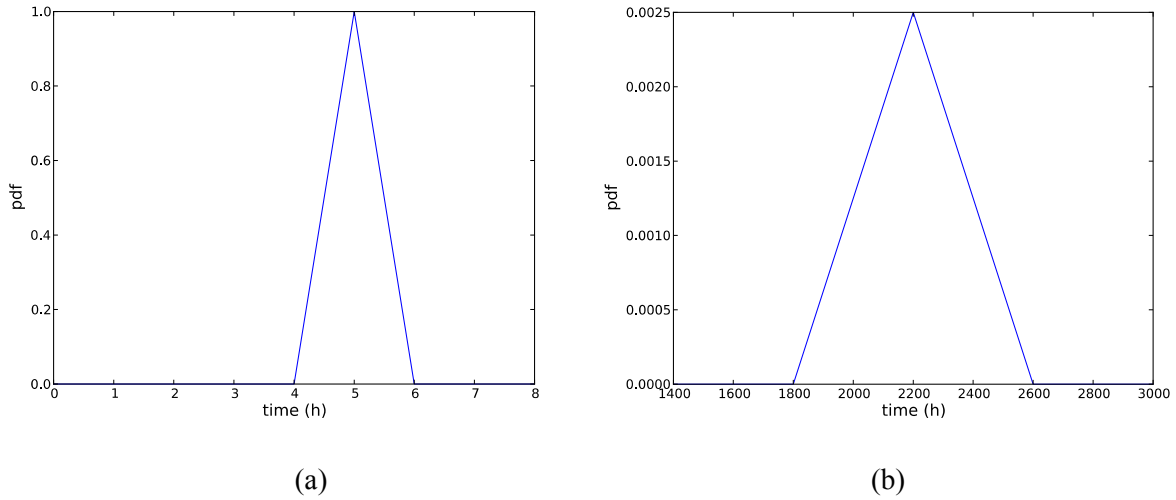


Figure 15: Plot of the pdfs of battery life (a) and clad failure temperature (b)

- **RCIC fails to run:** Regarding the distribution of RCIC to fail to run we assumed an exponential distribution $4.43 \cdot 10^{-3}$ as indicated in the SPAR model (see Figure 16).

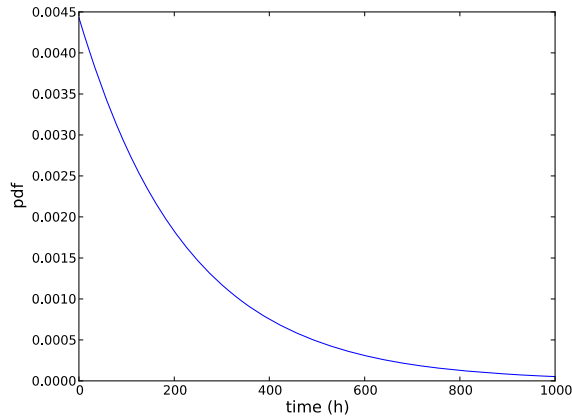


Figure 16: Plot of the pdf of RCIC and HPCI failure time

- **HPCI fails to run:** Identical distribution for RCIC fails to run distribution (see above)
- **Firewater flow rate:** The value of firewater flow rate is between 150 and 300 gpm [20]. For the scope of this report we also considered the possibility of very low firewater flow rates. Thus we assumed a triangular distribution defined in the interval [0,300] gpm with mode at 200 gpm (see Figure 17).

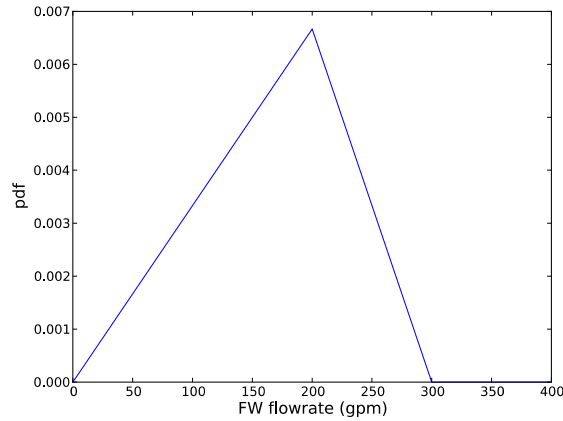


Figure 17: Plot of the pdfs of firewater flow rate

Regarding the pdfs related to human related actions we looked into the SPAR-H [21] model contained in SAPHIRE. SPAR-H characterizes each operator action through eight parameters – for this study we focused on the two important factors:

- Stress/stressors level
- Task complexity

These two parameters are used to compute the probability that such action will happen or not; these probability values are then inserted into the ETs that contain these events. However, from a simulation point of view we are not seeking if an action is performed but rather when such action is performed. Thus, we need a probability distribution function that defines the probability that such action will occur as function of time.

Since modeling of human actions is often performed using lognormal distributions [16], we chose such a distribution where its characters parameters (i.e., μ and σ) that are dependent on the two factors listed above (Stress/stressors level and Task complexity). We used Table 1 [15] to convert the three possible values of the two factors into numerical values for μ and σ .

Table 1: Correspondence table between complexity and stress/stressor level and time values

Complexity	μ (min)	Stress/stressors	σ (min)
High	45	Extreme	30
Moderate	15	High	15
Nominal	5	Nominal	5

For our specific case we modeled two human related actions as indicated below:

- **Battery repair time:** DC battery system restoration is performed by recovering batteries from nearby vehicles and connecting them to the plant DC system. We assumed that this task has high complexity with extreme stress/stressors level. This leads to $\mu = 45 \text{ min}$ and $\sigma = 15 \text{ min}$ (see Figure 18 a)

- **Firewater availability time:** The operations to align the firewater system to the RPV are considered a very complex operation. This time is measured after the ADS has been activated, i.e., after the RPV has been depressurized. Also for this case we assumed that this task has a high complexity with extreme stress/stressors level. This leads to $\mu = 45 \text{ min}$ and $\sigma = 30 \text{ min}$ (see Figure 18 b)

A summary of the distribution used is shown in Table 2.

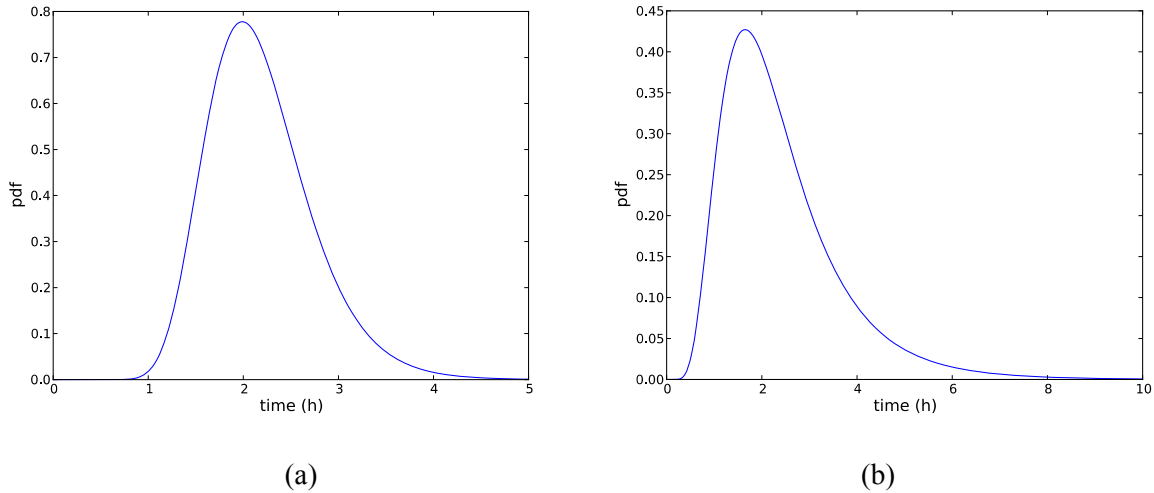


Figure 18: Plot of the pdfs for battery recovery time (a) and firewater availability time (b)

Table 2: Summary of the stochastic parameters and their associated distributions

No.	Stochastic variable*	Distribution type	Distribution parameters
1	Failure time of DGs (h)	Exponential	$\lambda = 1.09 \cdot 10^{-3}$
2	Recovery time of DGs (h)	Weibull	$\alpha = 0.745$ and $\beta = 6.14$
3	Battery life (h)	Triangular	(4, 5, 6)
4	SRV 1 fails open time	Bernoulli	$p = 8.56 \cdot 10^{-4}$
5	Offsite AC power recovery (h)	Lognormal	$\mu = 0.793$ and $\sigma = 1.982$
6	Clad Fail temperature (F)	Triangular	(1800, 2200, 2600)
7	HPCI fails to run (h)	Exponential	$\lambda = 4.43 \cdot 10^{-3}$
8	RCIC fails to run (h)	Exponential	$\lambda = 4.43 \cdot 10^{-3}$
9	Battery failure time (h)	Exponential	$\lambda = 3.5 \cdot 10^{-6}$
10	<i>Battery recovery time (min)</i>	Lognormal	$\mu = 45$, $\sigma = 15$
11	<i>Firewater availability time (min)</i>	Lognormal	$\mu = 45$, $\sigma = 30$
12	Firewater flow rate (gpm)	Uniform	(0, 200, 300)

* - Parameters related to human operations are in *italics*

3.5 RESULTS

In [16] we presented several analyses which included limit surface evaluations and uncertainty quantifications using advanced data analysis and data visualization techniques. In this report we focused

more on the probabilistic side of the analysis. Section 3.5.1 shows in fact how core damage probability, given a LOOP event, changes due to a power uprate. Section 3.5.2 shows some additional limit surface analyses given the updated BWR model.

3.5.1 STOCHASTIC ANALYSIS

We performed two series of Latin Hypercube Sampling analysis for the two levels of reactor power (100% and 120%) using 10,000 samples for each case. The scope of this analysis is to evaluate how CD probability changes when reactor power is increased by 20%. We also performed this comparison by identifying importance of specific events by performing the following for each case:

1. Building an ET based logic structure that queries the following events: SRV status, DG, PG and FW recovery (see Figure 19)
2. Associate each of the 10,000 simulations to a specific branch of the ET by querying the status of the SRV, PG, DG and FW components in the simulation run
3. Evaluate the probability and the outcome associated to each branch

A summary of the core damage probability for the cases is shown in Table 3: the probability value almost doubled for a 20% power increase. The summary of the branch probabilities represented in Figure 19 is shown in Table 4. As expected, all branches that lead to CD have a probability increase while the ones leading to OK decrease.

Table 3: Core damage probability for two different power levels (100% and 120%)

Outcome	100%	120%
OK	0.9902	0.9804
CD	9.82 E-3	1.95 E-2

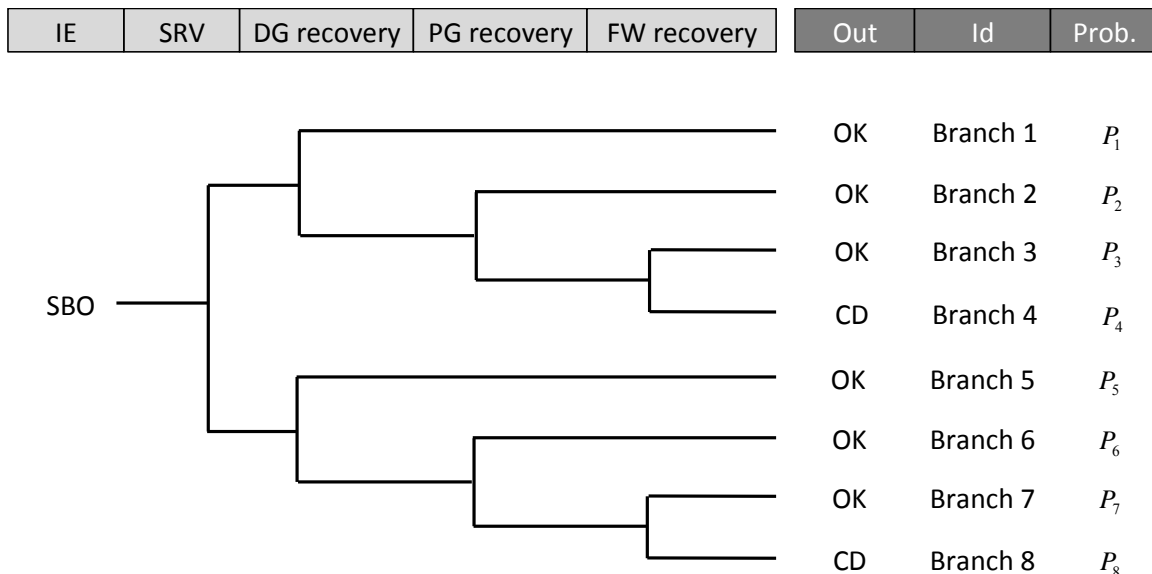


Figure 19: Simplified ET logic structure for a BWR SBO

Table 4: Branch probabilities associated to the ET shown in Figure 19 for both cases (100% and 120% power level)

Branch	Outcome	100%		120%		ΔP (%)
		Count	Probability	Count	Probability	
1	OK	3146	0.375	3238	0.353	-6
2	OK	4549	0.618	4440	0.606	-2
3	OK	847	0.00931	985	0.00926	-0.6
4	CD	557	0.00982	691	0.0196	+99
5	OK	333	7.32E-06	223	6.29E-06	-14
6	OK	254	1.53E-05	189	3.96E-06	-74
7	OK	251	5.92E-06	175	2.39E-06	-60
8	CD	63	2.12E-06	59	2.54E-06	+20

Regarding the FW flow rate, we were able to determine that a minimum value of 50 gpm is enough to assure an OK outcome. Note that branches 4 and 8 (in Figure 19) include also the simulations characterized by FW align before CD condition is met but with FW flow rate insufficient to keep the core cooled.

For the scope of this report, we focused on a safety relevant case: DG failure time vs. DG recovery time as shown in Figure 20. These limit surfaces are obtained using Support Vector Machines (SVM) based algorithms as shown in Appendix A.

As expected the failure region (red area) is expanding when reactor power is increased by 20%. This power increase on average reduces AC recovery time by about one hour.

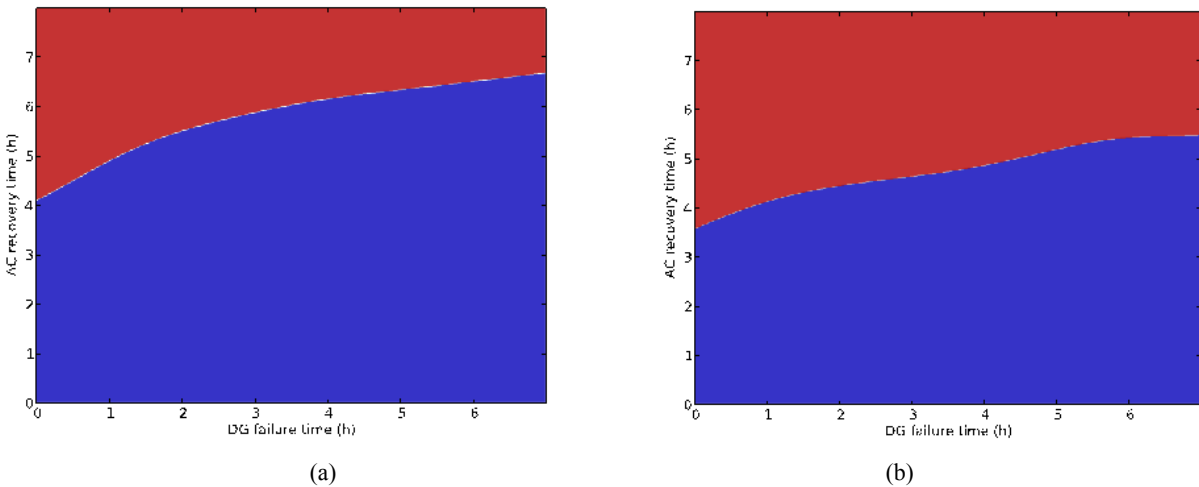


Figure 20: Limit surface obtained in a two dimensional space (DG failure time vs. AC recovery time) for two different power level: 100% (left) and 120% (right)

3.5.2 IMPACT OF AUXILIARY AC POWER SYSTEMS (FLEX SYSTEM)

In addition to the analysis reported above we evaluated the impact of auxiliary AC system generators as additional sources of AC power. The U.S. nuclear industry, as a measure after the Fukushima accident [22], developed a FLEX system to counterattack the risks associated with external events (e.g., earthquakes or flooding). Such a system employs portable AC and DC emergency generators located not only within the plant perimeter but also at strategic locations within the US borders in order to quickly supply affected NPPs with both AC and DC power.

For our case, we assumed a new distribution associated with the AC recovery time within the plant instead of the DG recovery time distribution. Since FLEX operations can be considered as human-related events, we followed the same approach described in Section 3.4 for human related events (see Table 1). In fact, we assumed that the AC recovery can be considered to be of moderate complexity and high levels of stress/stressors. Note that this model may not be indicative of any actual NPP FLEX strategies – for an actual FLEX evaluation, plant specific information would need to be considered. The new AC recovery distribution that replaces the DG recovery distribution is then a lognormal having a mean and a standard deviation values as follows (see Figure 21):

- mean = 15.0
- standard deviation = 15.0

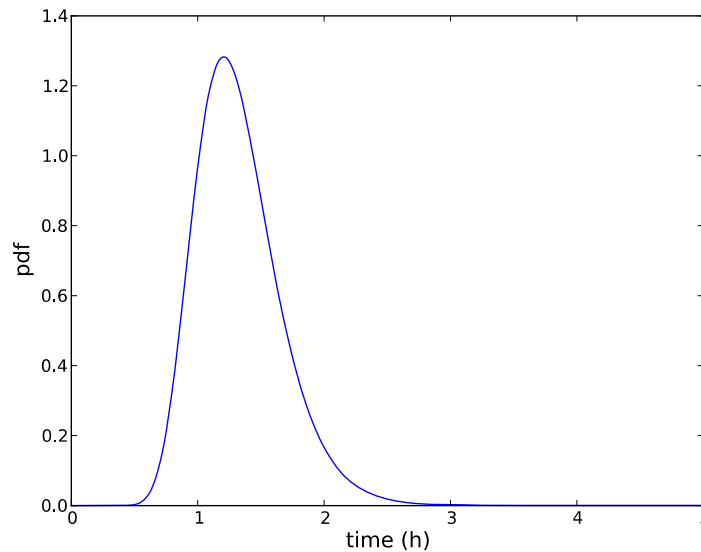


Figure 21: Plot of pdf for AC power recovery using FLEX system (to be compared with the pdf plotted in Figure 14)

Similarly to the analysis performed in Section 3.5.1, we performed a new Latin Hypercube Sampling analysis in order to estimate the new core damage probability value and the branch probabilities associated with the ET structure shown in Figure 19.

Table 5: Core damage probability for two different test cases (120% with and without FLEX system)

Outcome	120% w/o FLEX	120% w/ FLEX
OK	0.981	0.995
CD	1.95 E-2	4.59 E-3

Table 6: Branch probabilities associated to the ET shown in Figure 19 for two different test cases (120% with and without FLEX system)

Branch	Outcome	Probability (120%)		ΔP (%)
		w/o FLEX	w/ FLEX	
1	OK	0.353	0.505	43
2	OK	0.606	0.490	-21
3	OK	0.00926	3.49E-05	-100
4	CD	0.0196	0.00459	-77
5	OK	6.29E-06	2.87E-06	-54
6	OK	3.96E-06	1.79E-09	-100
7	OK	2.39E-06	6.77E-10	-100
8	CD	2.54E-06	1.09E-09	-100

As second step in the analysis, we focused on the concept of limit surfaces: the boundaries in the space of the sample parameters that separate failure from success. The advantage of limit surfaces is that they allow us to physically visualize how system performances are reduced due to, for example, a power uprate. By system performance, we mainly refer to both reduction in recovery timings (e.g., AC power recovery) and time reduction to perform steps in reactor operating procedures (e.g., time to reach HCTL).

4. CLASSICAL PRA COMPARED TO A SIMULATION-BASED APPROACH

In this section we describe a comparative analysis between RISMC approach described in detail in Section 3 with traditional risk analysis modeling for a BWR SBO accident scenario. Regarding the first approach, it is summarized in Section 4.1 while the classical EF-FT approach analysis using SAPHIRE is shown in detail in Section 4.2. Results are indicated in Section 4.3.

4.1 BWR SIMULATED DATA

The accident scenario under consideration is a LOOP initiating event followed by loss of the diesel generators (DGs), i.e., a SBO initiating event (see Figure 22). At time $t = 0$ the following events occur: LOOP condition occurs due to external events (i.e., power grid related), LOOP alarm triggers the following actions:

- Operators successfully scram the reactor
- Emergency DGs successfully start
- Core decay heat is removed from the reactor vessel
- DC systems (i.e., batteries) are functional

As part of the scenario, plant operators start recovery operations to bring back on-line the DGs while the recovery of the power grid is underway by the grid owner emergency staff. However, due to the limited life of the battery system and depending on the use of DC power, battery power can deplete. When this happens, all remaining control systems are offline causing the reactor core to heat until clad failure temperature is reached, i.e., core damage CD.

If DC power is still available and one of three specific conditions are reached, then the reactor operators activate the ADS system in order to depressurize the reactor.

As an emergency action, when reactor pressure is below 100 psi, plant staff can connect the firewater system in order to cool the core and maintain an adequate water level. However, this task is difficult to complete since the physical connection between the firewater system and the reactor vessel inlet has to be made manually.

When AC power is recovered, through successful re-start/repair of DGs or off-site power, reactor core cooling can be restored.

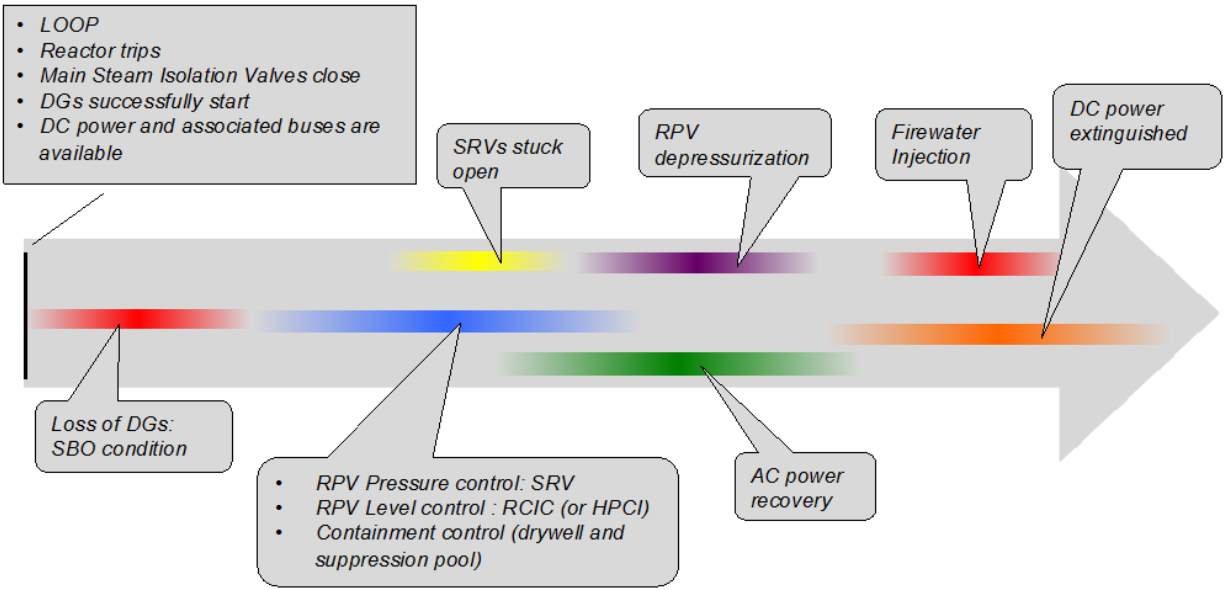


Figure 22: BWR SBO simulated data: sequence/timing of events

The choice of the set of stochastic parameters to consider in the analysis was based on the preliminary PRA model results obtained for a typical BWR SBO case. For all basic events (e.g., DG fail to run) we have considered the following sensitivity indexes common to PRA: the Fussell-Vesely and Birnbaum importance and a typical event-tree structure for a LOOP-SBO.

The probabilistic modeling of the possible human interventions was done by looking at the SPAR-H [21] model from a generic BWR PRA. In this respect, we have identified three actions:

- Manual activation of the automatic depressurization system: operator manually depressurizes the reactor by activation of the automatic depressurization system
- Extended ECCS operation: operators may extend RCIC/HPCI and SRVs control even after the batteries have been depleted. This action actually summarizes two events: manual control of RCIC/HPCI by acting on the steam inlet valve of the turbine and obtain DC power availability through spare batteries
- Firewater injection availability time (measured after depressurization has been activated)

SPAR-H characterizes each operator action through eight parameters – for this study we focused on two important factors:

- Stress/stressors level
- Task complexity

These two parameters are used to compute the probability that such action will happen or not; these probability values are then inserted into the event-trees that contain these events. However, from a simulation point of view we are not seeking *if* an action is performed but rather *when* such action is

performed. Thus, we need a probability distribution function that defines the probability that such action will occur as function of time.

Since modeling of human actions is often performed using lognormal distributions [16], we chose these distributions where its characteristic parameters (i.e., μ and σ) are dependent on the two factors listed above (Stress/stressors level and Task complexity). We used Table 7 [15] to convert the three possible values of the two factors into numerical values for μ and σ .

Table 7: Correspondence table between complexity and stress/stressor level and time values

Complexity	μ (min)	Stress/stressors	σ (min)
High	45	Extreme	30
Moderate	15	High	15
Nominal	5	Nominal	5

A summary of the stochastic parameters and their associated distributions is shown in Table 8.

The stochastic analysis for the BWR SBO test case has been performed using the code RAVEN [5] that is being developed by INL. Originally, RAVEN was designed to control the code RELAP-7, but its capabilities have been extended to include also stochastic analysis methodologies such as Monte-Carlo and Dynamic Event Tree algorithms.

In addition, RAVEN has been coupled to RELAP5-3D and RELAP-7 in order to perform multiple RELAP runs (through Monte-Carlo sampling). To evaluate the impact of the uncertain parameters summarized in Table 8 on the simulation outcome, we performed an extensive Monte-Carlo analysis that consisted of generating 20,000 Monte-Carlo runs.

Table 8: List of stochastic parameters and their associated distribution

No.	Stochastic variable	Distribution	Distribution parameters
1	Failure time of DGs (h)	Exponential	lambda = 1.09 E-3
2	Recovery time of DGs (h)	Weibull	alpha = 0.745, beta = 6.14
3	Battery life (h)	Triangular	(4, 5, 6)
4	SRV 1 fails open time	Binomial	8.56 E-4
5	SRV 2 fails open time	Binomial	8.56 E-4
6	Offsite AC power recovery (h)	Lognormal	mu = 0.793, sigma = 1.982
7	Clad Fail temperature (F)	Triangular	(1800, 2200, 2600)
8	HPCI fails to run (h)	Exponential	lambda = 4.4E-3
9	RCIC fails to run (h)	Exponential	lambda = 4.4E-3
10	<i>Firewater availability time</i> (h)	Lognormal	mu = 45/60, sigma = 30/60
11	<i>Extended ECCS operation</i> (h)	Lognormal	mu = 45/60, sigma = 30/60
12	<i>Manual ADS activation</i> (h)	Lognormal	mu = 5/60, sigma = 15/60

Note the analysis presented in Section 3 is slightly different from the one presented in this section in terms of stochastic parameters chosen. This difference is due to the fact that here we performed a comparison of two analyses that query same stochastic parameters.

4.2 CLASSICAL PRA DATA

In traditional PRA, the BWR SBO case studied is modeled with the following ETs (see Figure 23) that are linked together with the transferring feature in SAPHIRE software [5]:

- LOOP: Loss of Offsite Power
- SBO: Station Black Out
- SBO-1: SBO with 1 SRV stuck open
- SBO-2: SBO with 2 or more SRVs stuck open
- SBO-OP: AC recovered ET

There are actually four LOOP event trees based on the cause or location of the LOOP event occurred: LOOP-GR (grid related), LOOP-PC (plant centered), LOOP-SC (switchyard centered), and LOOPWR (weather related). The four trees have identical structure and top events except the initiators. LOOPGR is used as the representative LOOP event tree in this analysis.

The LOOP-GR ET (see Figure 24) starts with a grid related LOOP as initiating event followed by a branch on the success/failure of the reactor shutdown. Then the ET queries the status of emergency power (i.e., diesel generators). Success of reactor shutdown but failure of diesel generators (Sequence 28 of LOOP-GR) leads to a transfer ET: the SBO ET.

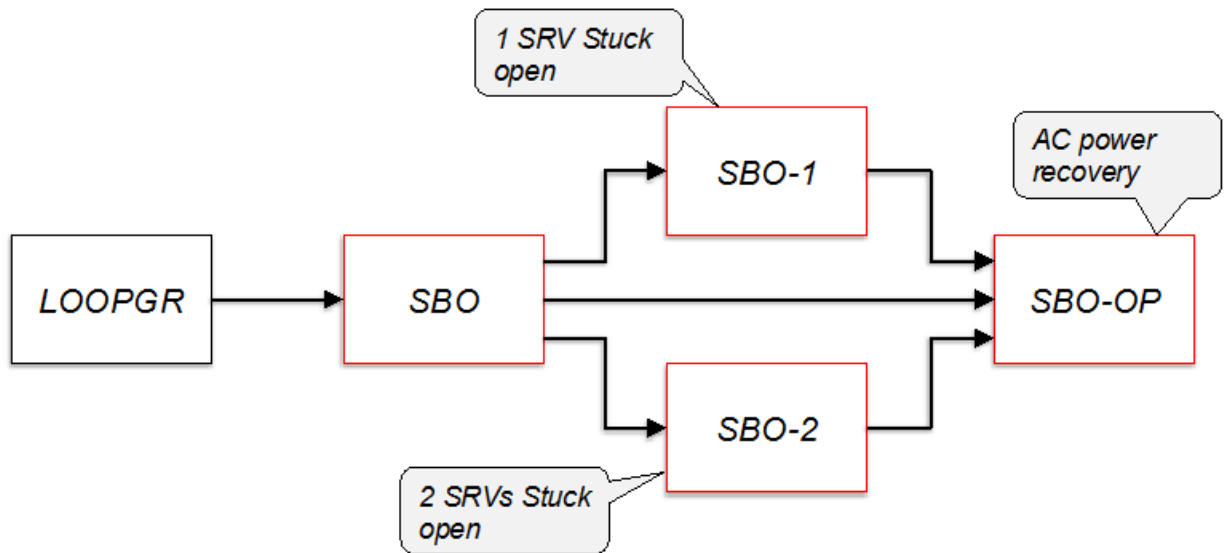


Figure 23: ET structure for the BWR SBO model contained in SAPHIRE

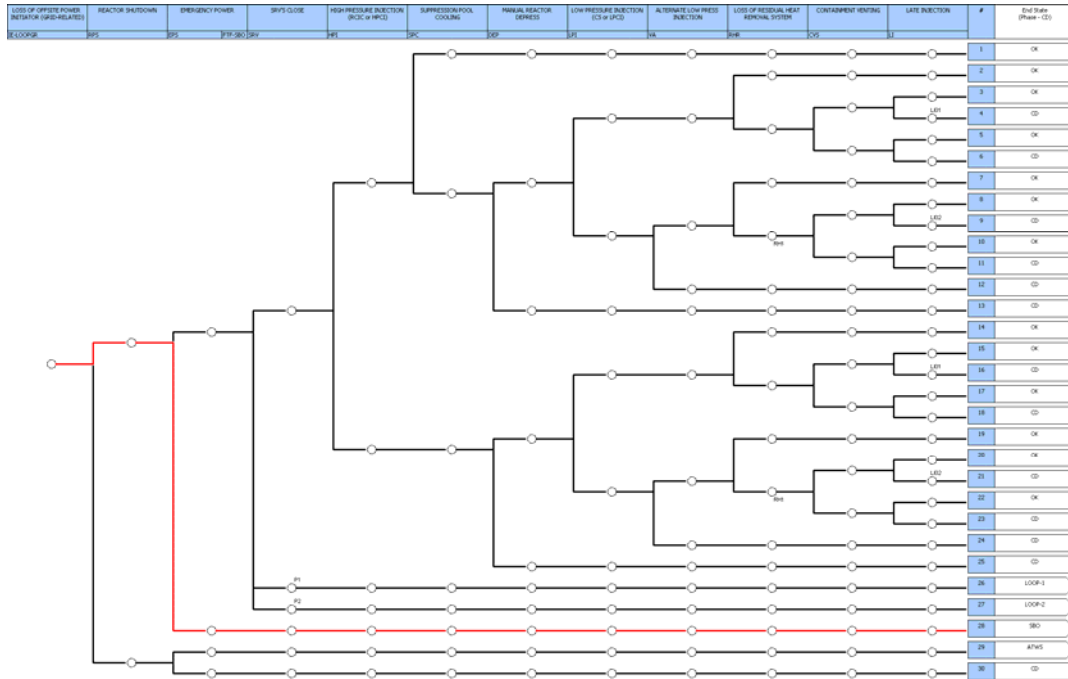


Figure 24: ET structure for LOOP grid related; red path is characterized by the loss of DGs and leads to the SBO ET (see Figure 25)

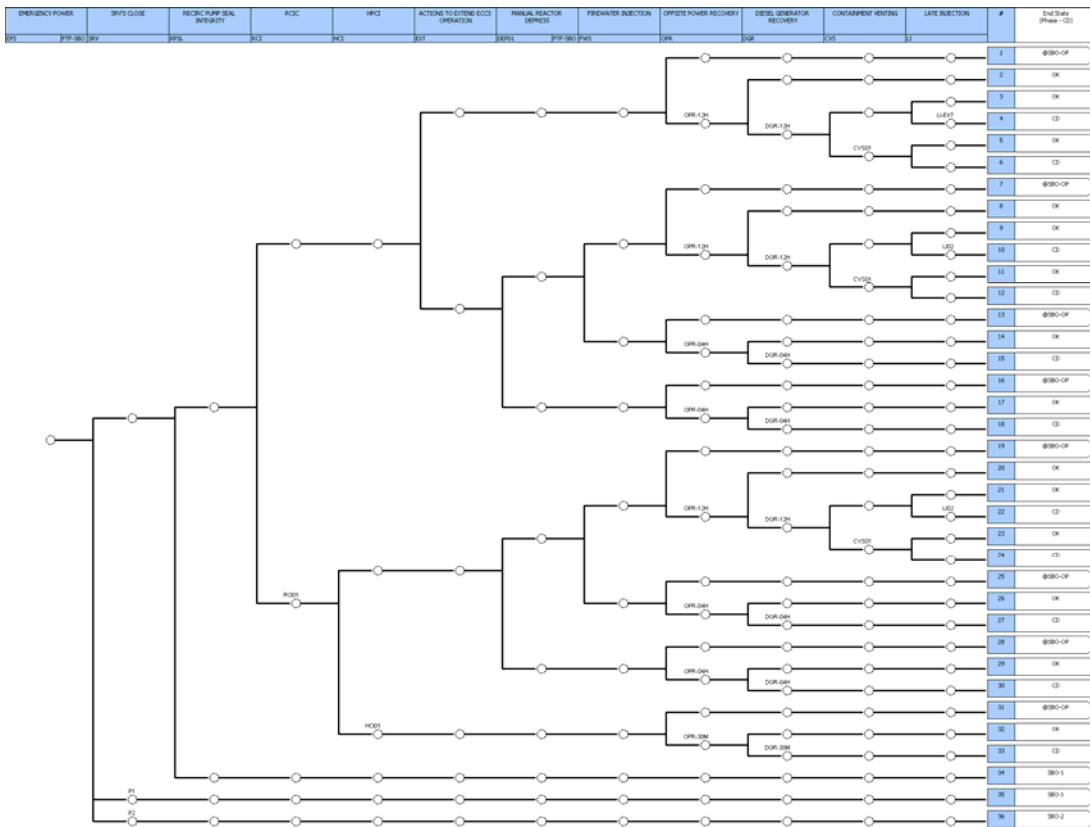


Figure 25: ET structure for SBO

In the SBO ET (see Figure 25) the following events are queried with a total of 36 sequences:

1. SRV(s) status: one stuck open SRV sequence (Sequence 35 of SBO) leads to another transfer ET: SBO-1. Two or more stuck open SRVs sequence (Sequence 36 of SBO) leads to the SBO-2 ET.
2. Recirculation pump seal integrity: failure of the recirculation pump (Sequence 34 of SBO) leads to the SBO-1 ET.
3. RCIC availability
4. HPCI availability
5. Extended ECCS operation
6. ADS activation
7. FW injection
8. Offsite power recovery
9. DG recovery
10. Containment venting
11. Late injection

In case one SRV (see Figure 26) or two or more SRVs (see Figure 27) are stuck open the following events are queried in sequence:

1. RCIC availability
2. HPCI availability
3. Offsite power recovery
4. DG recovery

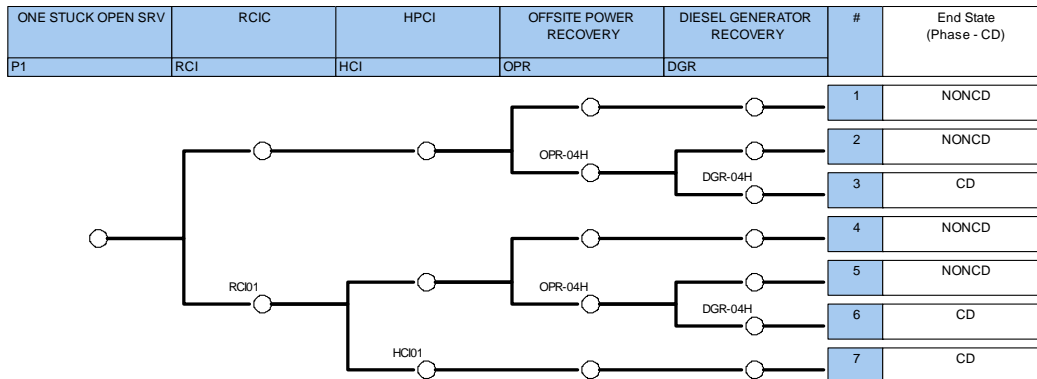


Figure 26: ET structure for one SRV stuck open

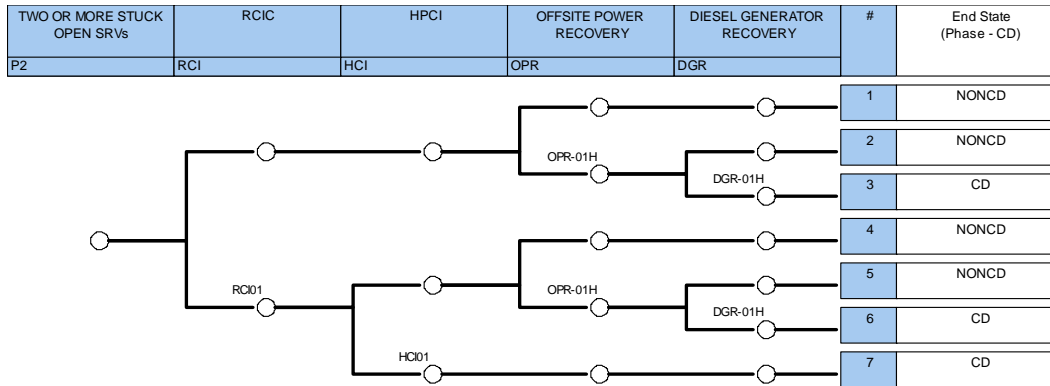


Figure 27: ET structure for two SRVs stuck open

To compare the RELAP/RAVEN simulation run results with the above traditional PRA models, all of the SBO sequences (including the sequences transferred to SBO-1 and SBO-2, whether they end with CD or non CD) have to be quantified. Note that this is different from the general Level 1 PRA quantification process in which only core damage sequences are quantified. Conditional sequence probability (versus conditional core damage probability, or CCDP, in general PRA quantification) given a SBO event occurred is used as the matrix of merit for the comparison.

In order to quantify non-core damage sequences as well as core damage sequences correctly, the impact of success branch probabilities of the ET top events must be considered. Two different approaches could be used to account for the probability of success branches by using what is known in SAPHIRE as the “process flag” feature. The results of both approaches must be post-processed to provide correct sequence frequency or conditional probability [23].

- In the developed event approach which uses the “W” process flag, SAPHIRE explicitly includes the success branch probability in the sequence cut sets. The event tree top event is treated as a basic event for the success branch and the complement of the event is used as the branch probability. However, this approach may contain non-coherent cut sets that should be reviewed, identified, and removed from the quantification results.
- In the other approach that uses the default, or blank, process flag, SAPHIRE uses a “delete term process” to prune success cut sets from the failure cut sets to generate coherent sequence cut sets. Success branch probabilities are not included in the sequence cut sets and must be manually added to be accounted for when the impact is not negligible. For example, offsite power recovery within 12 hours (OPR-12H) has a failure probability of 2.04E-2. Using the default process flag and delete term approach without accounting for its success probability (9.8E-1) may have only very small impact on the associated sequences (Sequences 1, 7, and 19 of the SBO ET) results. But for offsite power recovery within 30 minutes (OPR-30M), the failure probability is 8.63E-1 and the success probability is 1.37E-1. Without accounting for this success branch probability would increase the value of Sequence 31 of the SBO event tree by 8 times.

Table 7 presents the BWR SBO PRA model quantification results. Note that using the “W” process flag or using the default process flag without adjusting the results with the success branch probabilities yields incorrect results with a total conditional probability greater than 1.0. The last column, using the default process flag and adjusting the results with the success branch probabilities, shows correct conditional probabilities for SBO sequences that will be used for the comparison in Section 4.3.

For our application scope, no failures/events occur between the LOOP and the Loss of DGs; thus we did not consider the initial ET (i.e. LOOPGR). In addition, in the RELAP5-3D simulations we did not account for failures followed after AC power recovery; hence the event tree SBO-OP was not considered.

Table 9: SBO sequence quantification results for a typical BWR PRA model

SBO Model Sequence	Sequence End State	Conditional Sequence Probability ("W" Process Flag) ¹	Conditional Sequence Probability (Default Process Flag, Not Adjusted) ²	Conditional Sequence Probability (Default Process Flag, Adjusted) ³
1	Non-CD	5.93E-01	1.00E+00	5.92E-01
2	Non-CD	6.62E-03	2.04E-02	6.60E-03
3	Non-CD	2.92E-03	9.50E-03	2.92E-03
4	CD	1.21E-03	2.31E-03	9.77E-04
5	Non-CD	1.26E-03	2.87E-03	1.26E-03
6	CD	5.21E-04	6.98E-04	4.22E-04
7	Non-CD	1.73E-01	2.35E-01	1.40E-01
8	Non-CD	2.05E-03	5.10E-03	1.67E-03
9	Non-CD	1.24E-03	2.37E-03	1.01E-03
10	CD	0.00E+00	0.00E+00	0.00E+00
11	Non-CD	5.37E-04	7.17E-04	4.38E-04
12	CD	0.00E+00	0.00E+00	0.00E+00
13	Non-CD	4.86E-02	8.07E-02	4.82E-02
14	Non-CD	3.00E-03	1.38E-02	3.00E-03
15	CD	6.94E-03	9.66E-03	6.94E-03
16	Non-CD	3.04E-02	4.34E-02	3.03E-02
17	Non-CD	1.88E-03	7.40E-03	1.87E-03
18	CD	4.34E-03	5.17E-03	4.34E-03
19	Non-CD	4.07E-02	6.70E-02	4.04E-02
20	Non-CD	4.60E-04	1.40E-03	4.61E-04
21	Non-CD	2.79E-04	6.50E-04	2.79E-04
22	CD	0.00E+00	0.00E+00	0.00E+00
23	Non-CD	1.21E-04	1.96E-04	1.21E-04
24	CD	0.00E+00	0.00E+00	0.00E+00
25	Non-CD	6.46E-03	1.07E-02	6.44E-03
26	Non-CD	3.96E-04	1.81E-03	3.96E-04
27	CD	9.17E-04	1.27E-03	9.20E-04
28	Non-CD	6.88E-03	9.78E-03	6.87E-03
29	Non-CD	4.21E-04	1.65E-03	4.21E-04
30	CD	9.76E-04	1.15E-03	9.72E-04
31	Non-CD	5.14E-04	4.16E-03	5.12E-04
32	Non-CD	2.65E-04	3.59E-03	2.65E-04
33	CD	2.97E-03	3.30E-03	2.97E-03

SBO Model Sequence	Sequence End State	Conditional Sequence Probability ("W" Process Flag) ¹	Conditional Sequence Probability (Default Process Flag, Not Adjusted) ²	Conditional Sequence Probability (Default Process Flag, Adjusted) ³
34-1	Non-CD	7.75E-02	1.00E-01	7.75E-02
34-2	Non-CD	4.74E-03	1.69E-02	4.76E-03
34-3	CD	1.10E-02	1.18E-02	1.10E-02
34-4	Non-CD	5.34E-03	6.83E-03	5.34E-03
34-5	Non-CD	3.27E-04	1.15E-03	3.24E-04
34-6	CD	7.56E-04	8.05E-04	7.57E-04
34-7	CD	4.16E-04	4.17E-04	4.17E-04
35-1	Non-CD	6.64E-04	8.56E-04	6.64E-04
35-2	Non-CD	4.06E-05	1.44E-04	4.06E-05
35-3	CD	9.40E-05	1.01E-04	9.42E-05
35-4	Non-CD	4.58E-05	5.86E-05	4.58E-05
35-5	Non-CD	2.80E-06	9.87E-06	2.78E-06
35-6	CD	6.48E-06	6.89E-06	6.48E-06
35-7	CD	3.57E-06	3.57E-06	3.57E-06
36-1	Non-CD	6.09E-05	1.91E-04	6.08E-05
36-2	Non-CD	1.51E-05	1.26E-04	1.52E-05
36-3	CD	1.02E-04	1.10E-04	1.03E-04
36-4	Non-CD	4.20E-06	1.31E-05	4.20E-06
36-5	Non-CD	1.04E-06	8.62E-06	1.05E-06
36-6	CD	7.06E-06	7.51E-06	7.06E-06
36-7	CD	7.97E-07	7.97E-07	7.97E-07
Total		1.04E+00	1.68E+00	1.00E+00

Notes:

1. Using the "W" process flag leads to non-coherent cut sets in the results and a total conditional probability that is greater than 1.
2. Using the default process flag without adjusting the results with the success branch probabilities leads a total conditional probability that is greater than 1.
3. Using the default process flag and adjusting the results with the success branch probabilities yields correct sequence probabilities.

4.3 COMPARISON METHODOLOGY

In order to compare the results generated by RAVEN/RELAP5-3D (see Section 3.1) and traditional methods (see Section 3.2), we performed the following steps:

1. Merge the event trees SBO, SBO-1 and SBO-2 into a single event tree and recalculate branch probabilities (see Section 4.3.1)
2. Associate each of the 20,000 scenarios simulated using RELAP5-3D to a unique branch of the SBO ET built in Step 1. Perform a posteriori analysis for the scenarios that were not associated with an event tree branch (see Section 4.3.2)

3. Identify inconsistencies between RAVEN/ RELAP5-3D and the traditional approach in terms of outcome (e.g., core damage CD or system OK) and probabilities (see Section 4.4)

Note that a single branch of the event tree might contain several RELAP5-3D simulations.

4.3.1 ET RESTRUCTURING

A simplified SBO ET model (see Figure 28) was developed for more effective comparison between the simulation results and the PRA results. The total number of sequences is reduced from 54 (see Table 9) in the original SBO event tree model (including the SBO, SBO-1, and SBO-2 event trees) to 18 in the simplified event tree (see Table 10). The simplified event tree has the following top events:

1. SRV(s) status: no stuck open SRV, one stuck open SRV, or two or more stuck open SRVs.
2. High pressure injection (HPI) availability: HPI is success if either RCIC or HPCI is available.
3. Depressurization and firewater injection
4. Offsite power or DG recovery

Unlike the original SBO model, the simplified ET does not include the top event for recirculation pump seal integrity. Due to seal LOCA model instability, the RELAP5-3D /RAVEN simulation runs do not include the stochastic parameters related to the event and thus have no data to compare.

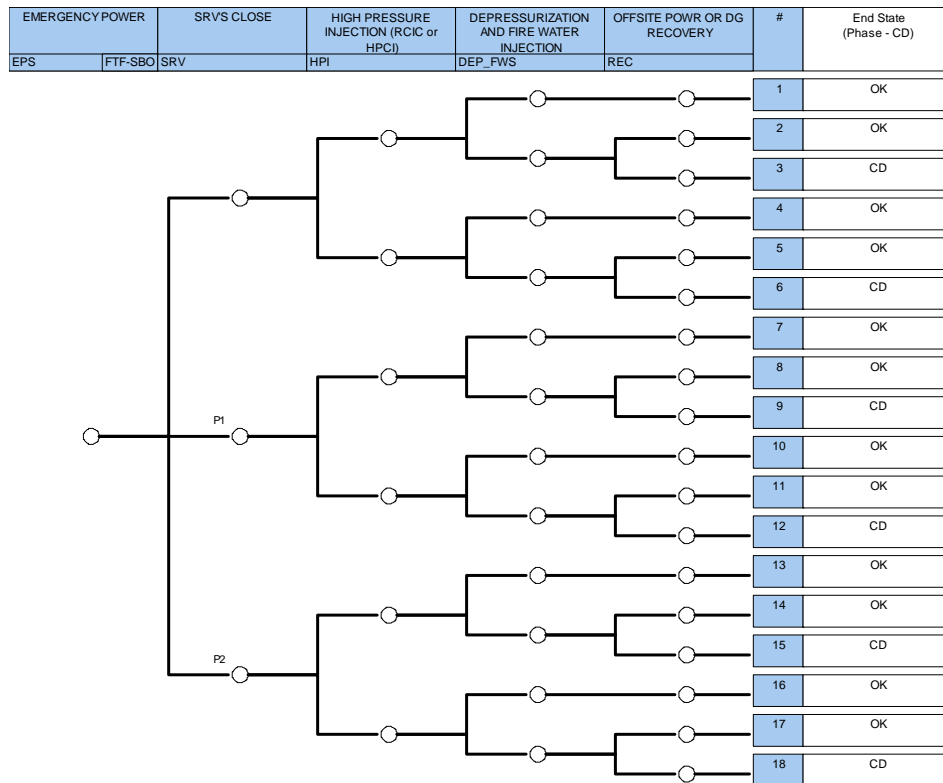


Figure 28: Simplified SBO ET model

Table 10 presents the 18 sequences in the simplified SBO event tree, the queried system status/functionalities for each sequence, the equivalent sequence(s) in the original SBO model, as well as the end state of each sequence. For example, Sequence 1 of the simplified event tree represents the scenarios in which no stuck open SRV, either HPCI or RCIC is successful, RCS depressurization and firewater injection are also successful (SRV0 * /HPI * /DEP_FWS). With the successful mitigation, there is no core damage (end state of OK). Sequences 3, 5, 7 to 12, and 19 to 24 in the original SBO model have the same characterization and can be classified into the same category. Another example is Sequence 3 of the simplified model – this sequence also has no stuck open SRV with either HPCI or RCIC being functional. But with no RCS depressurization and/or firewater injection and without AC power recovery (neither offsite power nor diesel generators), core damage cannot be prevented (end state of CD). In the original model, the counterpart sequences are Sequences 4, 6, 15, 18, 27, and 30.

Table 10: Simplified SBO model sequences versus original SBO model sequences

Sequence	SRV	Other Functions	Original Model Sequence	End State
1	SRV0 *	/HPI * /DEP_FWS	3 + 5 + Sum(7:12) + Sum(19:24)	OK
2		/HPI * DEP_FWS * /REC	1+2+13+14+16+17+25+26+28+29	OK
3		/HPI * DEP_FWS * REC	4 + 6 + 15 + 18 + 27 + 30	CD
4		HPI * /DEP_FWS	n/a ¹	OK
5		HPI * /REC	31 + 32	OK
6		HPI * REC	33	CD
7	SRV1 *	/HPI * /DEP_FWS	n/a ²	OK
8		/HPI * DEP_FWS * /REC	35-1 + 35-2 + 35-4 + 35-5	OK
9		/HPI * DEP_FWS * REC	35-3 + 35-6	CD
10		HPI * /DEP_FWS	n/a ²	OK
11		HPI * DEP_FWS * /REC	n/a ²	OK
12		HPI * DEP_FWS * REC	35-7	CD
13	SRV2 *	/HPI * /DEP_FWS	n/a ²	OK
14		/HPI * DEP_FWS * /REC	36-1 + 36-2 + 36-4 + 36-5	OK
15		/HPI * DEP_FWS * REC	36-3 + 36-6	CD
16		HPI * /DEP_FWS	n/a ²	OK
17		HPI * DEP_FWS * /REC	n/a ²	OK
18		HPI * DEP_FWS * REC	36-7	CD

Notes:

1. The original SBO model does not credit DEP_FWS due to short time window for operator actions with HPI failure.
2. For simplicity reason, the original SBO model does not model DEP_FWS in SRV stuck open sequences.

Note that there are a few sequences in the simplified ET that have no corresponding sequences in the original model. For Sequence 4 of the simplified event tree (no stuck open SRV, HPI failure, but depressurization and firewater injection are successful), the original SBO model does not credit the depressurization and firewater injection with the assumption that there is no adequate time for operator to depressurize RCS and align firewater system for injection. Sequences 7, 10, 11 (one stuck open SRV, depressurization and firewater injection success or failure) and Sequences 13, 16, and 17 (two or more stuck open SRV, depressurization and firewater injection success or failure) of the simplified event tree also have no corresponding sequences in the original SBO model as the depressurization and firewater injection are not modeled for stuck open SRV event trees (see SBO-1, SBO-2) for simplification reasons.

4.3.2 SIMULATED DATA PROCESSING

Step 3 of Section 4.3 was performed by using an ad-hoc built PYTHON script. Its task was to parse all 20,000 simulations and perform Step 3 by considering throughout the simulation the status of system of components queried in the BWR SBO traditional model. For each simulation run the following information are retrieved:

- SRVs status
- High pressure injection status (both RCIC and HPCI)
- FW status
- AC power status (either DG or PG)

This allows the program to uniquely match each simulation run with a single branch of the event-tree shown in Figure 28. The main idea is to create a set of information that is shared between the simulation data and the ET SBO generated by SAPHIRE. Once this information is filtered from each simulation run, the script associates each scenario to a single branch of the ET shown in Figure 28.

In addition, the script generate for each branch the following information as a summary of the simulations classified into that particular branch (see Figure 29):

- Number of scenarios classified
- Probability of all scenarios classified
- Histogram of the outcome (OK due to AC recovery, OK due to firewater availability, CD)
- Maximum temperature of the clad
- Simulation end time
- Time of DG failure
- Plot of temporal profile of selected variables
- Summary of sequencing of events

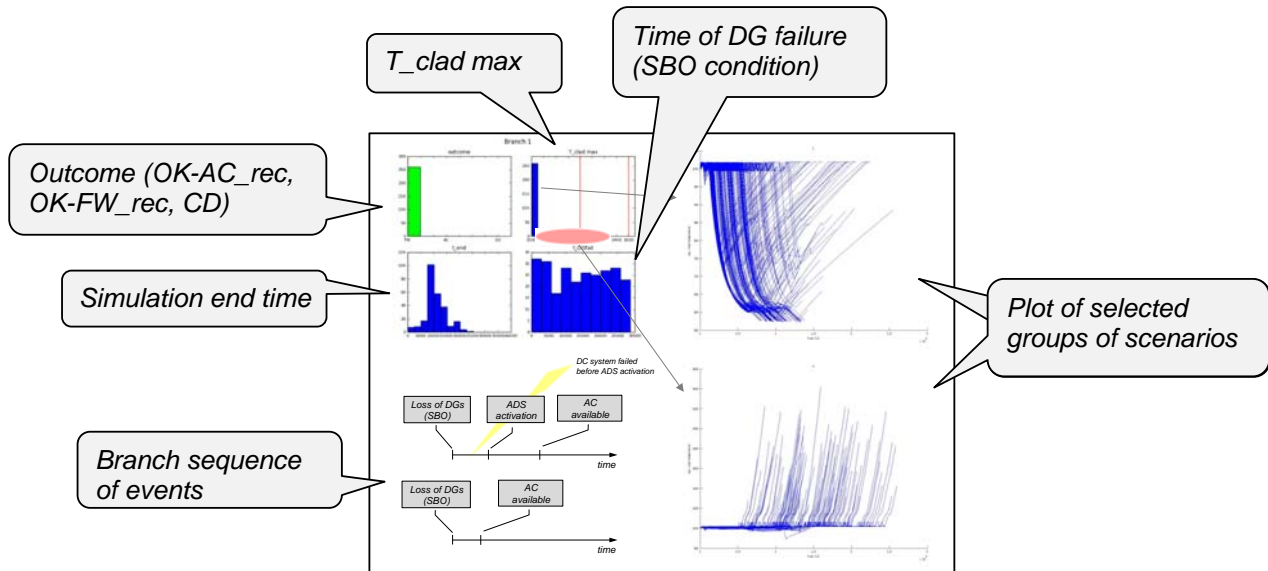


Figure 29: Output for each ET branch generated by the PYTHON script

4.4 COMPARISON RESULTS

After running the PYTHON scripts we note the following:

- Each of the 20,000 simulations were classified into a unique branch of the ET shown in Figure 28
- The outcome of each ET branch agrees with the final state of all simulations classified into that branch.

From Table 11 we can see the probability of CD for the simulations generated by RAVEN/ RELAP5-3D is fairly similar to the value generated by traditional methods (2.00 E-2 and 1.50 E-2 respectively). Core damage probability calculated using simulation based PRA (i.e., the RISMC approach) is 23% lower than one obtained using traditional ET/FT methods.

However, we noticed that, by looking at the probabilities associated with each event tree branch, some differences arise. Table 12 shows these differences for all 18 branches of Figure 28. In particular, we noticed that the distributions associated with the recovery time of AC power (either DGs or off site grid recovery), firewater recovery and SRV failure are driving these differences.

Table 11: Comparison of CD and OK probabilities

Methodology	OK	CD
Traditional	0.980	2.00 E-2
Simulation	0.985	1.54 E-2

Table 12: Comparison of sequences (i.e., branch) probabilities (refer to the ET of Figure 28)

<i>Branch no.</i>	<i>Outcome</i>	<i>Traditional</i>	<i>Simulation</i>
1	OK	0.21	0.10
2	OK	0.77	0.86
3	CD	0.017	0.010
4	OK	n/a*	0.021
5	OK	8.6E-04	0.0056
6	CD	0.0033	0.0050
7	OK	n/a**	9.9E-06
8	OK	8.2E-04	1.7E-06
9	CD	1.1E-04	2.1E-07
10	OK	n/a**	6.7E-07
11	OK	n/a**	9.7E-07
12	CD	4.0E-06	5.0E-07
13	OK	n/a**	9.5E-07
14	OK	8.9E-05	2.6E-07
15	CD	1.2E-04	1.8E-07
16	OK	n/a**	2.9E-07
17	OK	n/a**	4.3E-08
18	CD	9.6E-07	2.1E-08

Notes:

* - The original SBO model does not credit DEP_FWS due to short time window for operator actions with HPI failure.

** - For simplicity, the original SBO model does not model DEP_FWS in SRV stuck open sequences.

By looking at the histograms of the maximum clad temperature (see Figure 30), we were also able to determine that for the scenarios contained in branches leading to system OK, such histograms were containing scenarios with high clad temperatures. This fact was caused by a failure of the DC system but followed by AC recovery just before reaching CD.

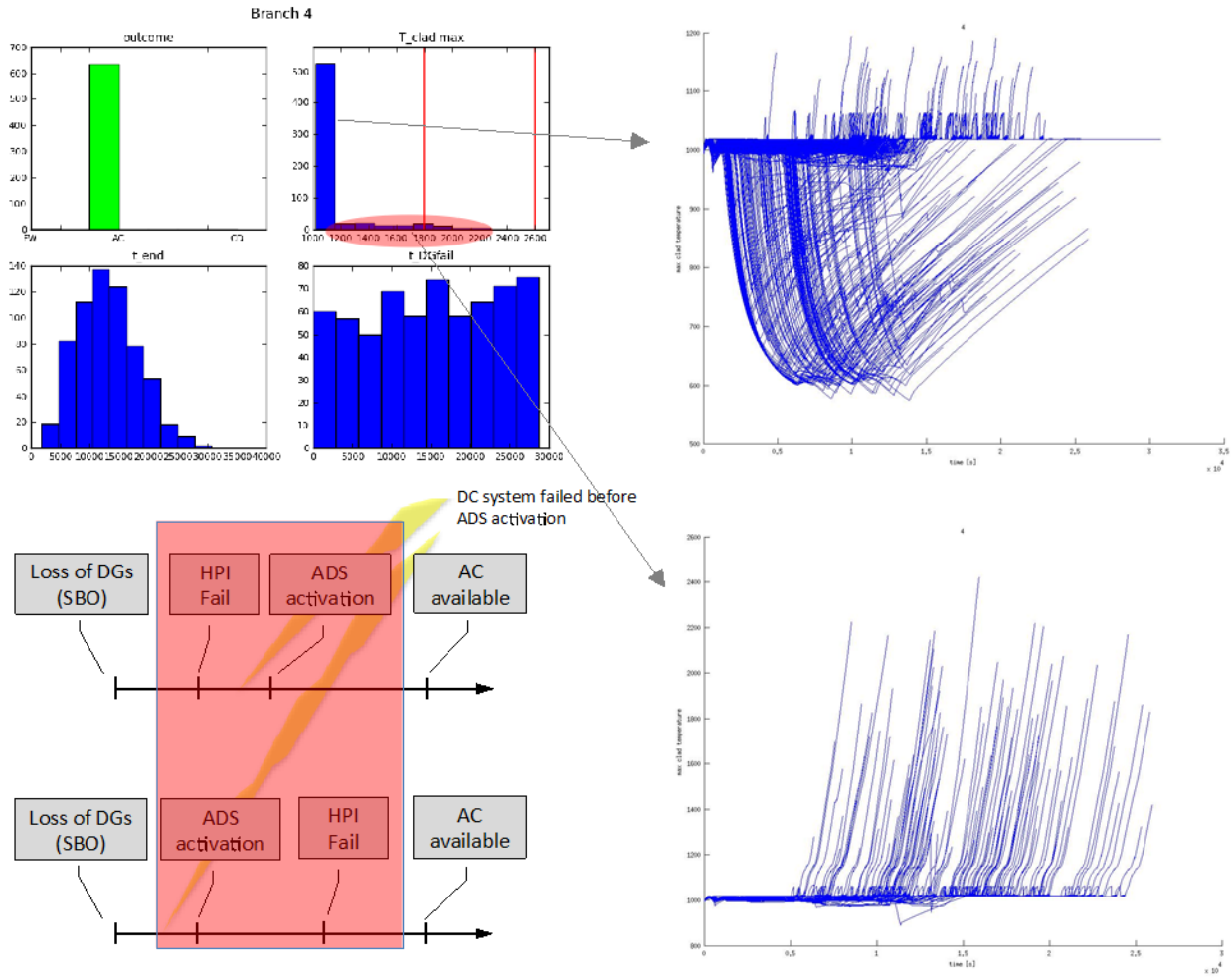


Figure 30: Effect of DC system failure on max clad temperature histogram for scenarios leading to system OK

5. RELAP5-3D AND RELAP-7 INITIAL COMPARISON

This section presents some of the preliminary analysis performed to compare the numerical results obtained using RELAP5-3D [4] and RELAP-7 [7]. Due to the fact that the two-phase capabilities of RELAP-7 are still under development, we focused on a system characterized by single-phase (i.e., water in liquid state) as described in Section 5.1. The comparison was performed not only from a steady state point of view but we also considered a simple transient as shown in Sections 5.2.1 and 5.2.2.

5.1 SYSTEM DESCRIPTION

The system considered is a 2-loop Pressurized Water Reactor (PWR) system as shown in Figure 31. The reactor vessel model consists of the Down-comers, the Lower Plenum, the Reactor Core Model and the Upper Plenum. Three Core-Channels (components with a flow channel and a heating structure) were used to describe the reactor core. Each Core-Channel is representative of a region of the core (from one to thousands of real cooling channels and fuel rods).

In this analysis, the core model consists of three parallel Core-Channels (hot, medium and cold) and one bypass flow channel. Respectively they represent the inner and hottest zone, the mid and the outer and colder zone of the core. The Lower Plenum and Upper Plenum are modeled with Branch models. Power fraction for each core channel is specified in Table 13.

There are two primary loops in this model – Loop A and Loop B. Each loop consists of the Hot Leg, a Heat Exchanger and its secondary side pipes, the Cold Leg and a primary Pump. A Pressurizer is attached to the Loop-A piping system to control the system pressure. Since a complex Pressurizer model has not been implemented yet in the current version of RELAP-7 code, a Time Dependent Volume (pressure boundary condition) has been used instead.

We built the input files that model the PWR model described above for both RELAP-7 and RELAP5-3D as shown in Figure 32 and Figure 33 respectively.

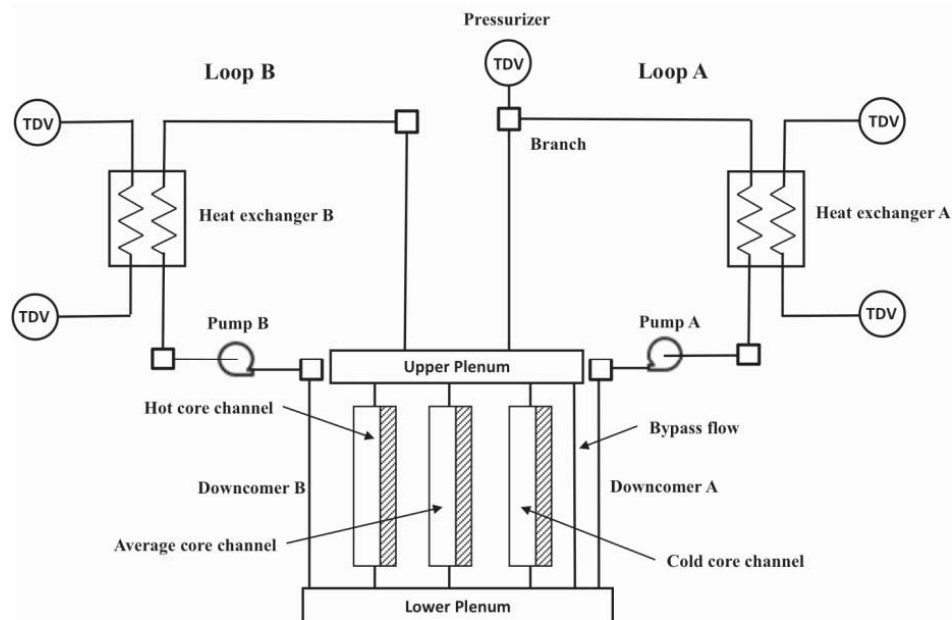


Figure 31: Scheme of the TMI PWR benchmark

Table 13: Power distribution factor for representative channels and average pellet power

Core Channel	Power Distribution Factor	Average fuel pellet power density (W/m^3)
Hot	0.3337	$3.90 \cdot 10^8$
Average	0.3699	$3.24 \cdot 10^8$
Cold	0.2964	$2.17 \cdot 10^8$

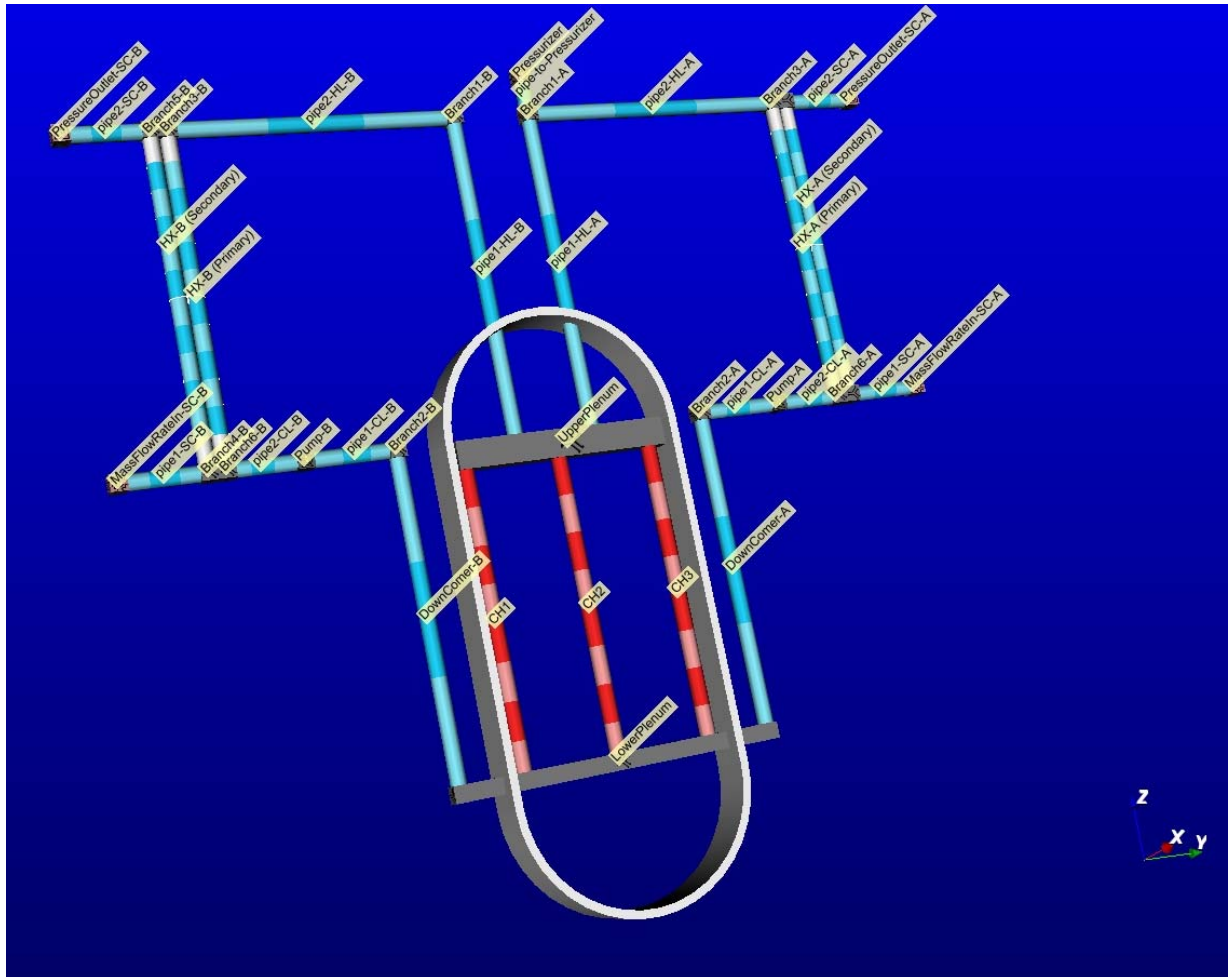


Figure 32: Screenshot of the PWR model of RELAP-7 using PEACOCK

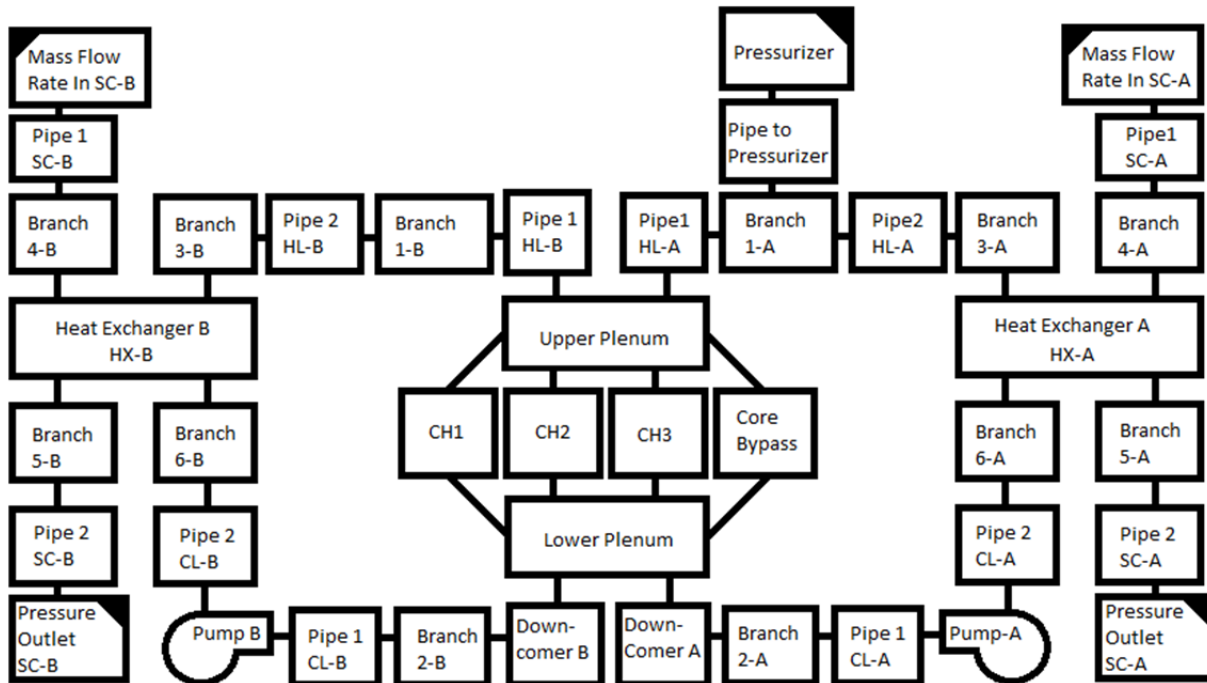


Figure 33: RELAP5-3D nodalization of the PWR model

To compare RELAP5-3D and RELAP-7, a second PWR model was prepared to be run with RELAP5-3D. This model was built to mimic the RELAP-7 PWR model as closely as possible. To this end, the RELAP5-3D model used, wherever possible, identical geometry to the RELAP-7 model.

A major difference between the two was that RELAP5-3D is incapable of junctions between more than two components – in RELAP5-3D, a junction must be between only two components. In RELAP-7, multi-connection junctions are possible, and were used. To replicate this in RELAP5-3D, the Branch component was used. RELAP5-3D’s Branch component can make connections to as many other components as needed, but does require an assigned area and length, where the RELAP-7 counterpart does not need a length. To compensate for this, after consulting with an INL RELAP5-3D expert, it was decided that any time a Branch was used in RELAP5-3D to replicate a RELAP-7 component with no assigned length, the RELAP5-3D component would be assigned to have no wall friction and no change in elevation. With no change in elevation and no wall friction, the length of the RELAP5-3D component became inconsequential. With no heat structure associated with these components, no wall friction, and no change in elevation, the only effect the component would have on the internal energy of the coolant would be through form loss. Given that the area of each RELAP5-3D component was the same as the area of its RELAP-7 counterpart, the form loss was expected to be identical.

A second difference between RELAP5-3D and RELAP-7 was that the RELAP-7 heat exchanger was replicated using multiple RELAP5-3D components. The RELAP-7 heat exchanger is a simple setup, and is essentially two pipes and a heat structure with the left boundary of the heat exchanger connected to one pipe, and the right boundary of the heat exchanger connected to the other pipe. Appropriately, this was replicated in RELAP5-3D with a heat structure and two pipes in an identical arrangement.

After initially coding the RELAP5-3D model, one major adjustment was made. The ‘Pump’ component in both of the two loops were removed and replaced with ‘Time-Dependent Junction’

components. This was done because in RELAP-7, ‘Ideal Pump’ components were used that, rather than providing any kind of pump head, are an idealized pump that provides a set, constant mass flow rate. This is done in RELAP5-3D using Time-Dependent Junction components, which can similarly provide a set, constant mass flow rate.

Additionally, after running the RELAP5-3D model, it was slightly tuned by lowering the input temperature to the heat exchanger on the secondary loop side of the heat exchanger. Results of both the tuned and un-tuned RELAP5-3D model are presented below, in comparison to the RELAP-7 results.

5.2 COMPARISON RESULTS

We performed two types of analyses, steady state and transient, that are reported in Sections 5.2.1 and 5.2.2 respectively.

5.2.1 STEADY STATE RESULTS

The plots of the steady state simulations for RELAP-7 and RELAP5-3D are shown in Figure 34 and Figure 35 respectively while Table 14 summarizes the average temperature reached in the three core channels.

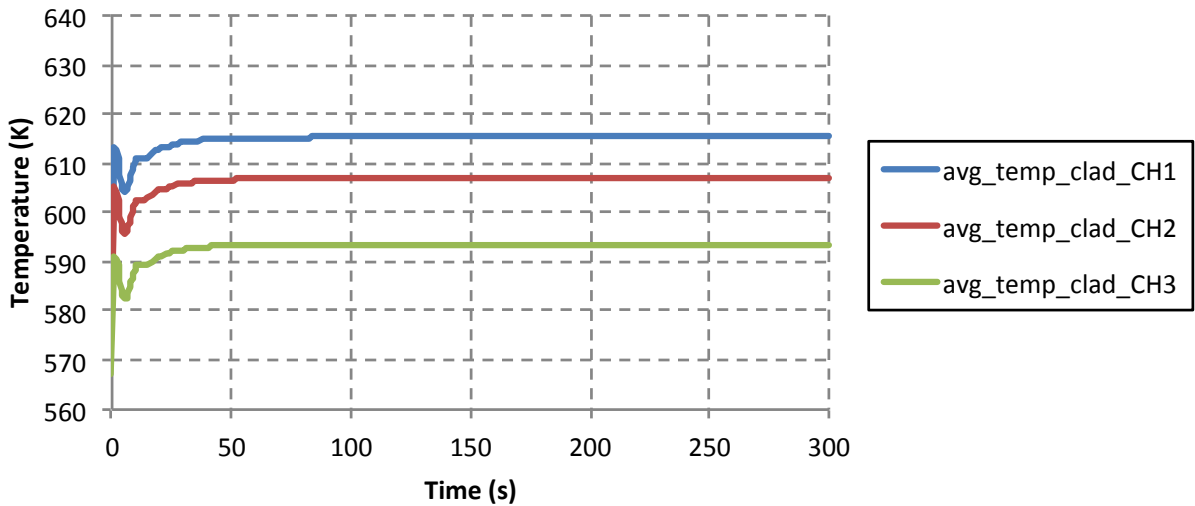


Figure 34: Steady state analysis for the simplified PWR model using RELAP-7

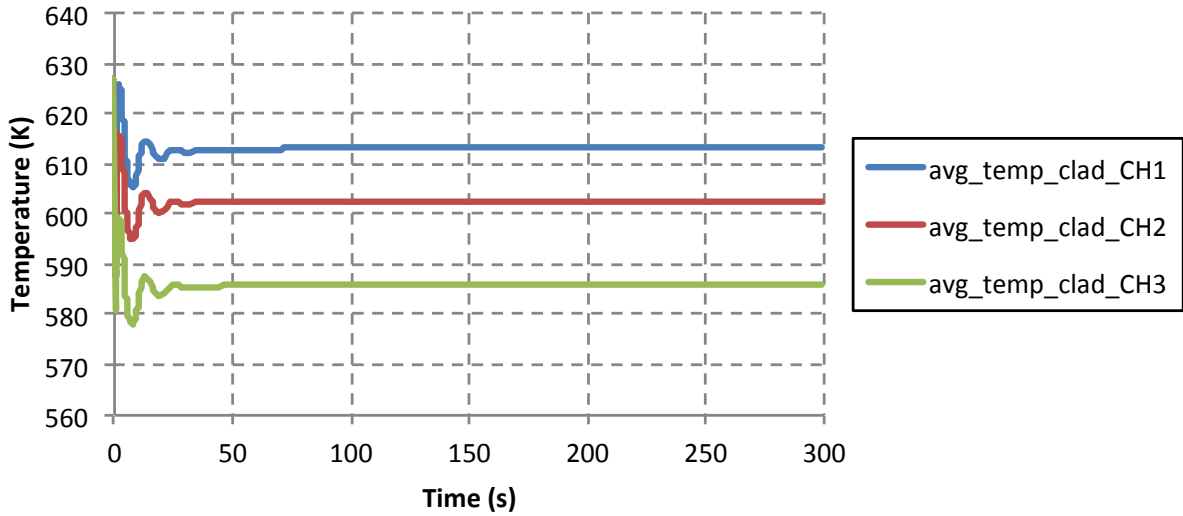


Figure 35: Steady state analysis for the simplified PWR model using RELAP5-3D

Table 14: Summary of the core channels average temperatures for RELAP5-3D and RELAP-7

<i>Code</i>	<i>Channel 1</i>	<i>Channel 2</i>	<i>Channel 3</i>
RELAP-7	615.3	606.9	593.5
RELAP5-3D	613.1	602.7	586.0

It is expected that the difference between the models was caused by approximations that RELAP-7 currently uses. Additionally, in RELAP-7, the convective heat transfer coefficient is dictated, where RELAP5-3D uses any of several predictive equations to determine the convective heat transfer coefficient.

Though the models do not agree perfectly, the original untuned RELAP5-3D model agrees fairly well with the RELAP-7 model, and the RELAP-7 predicted clad temperatures are within roughly 3% of the predicted untuned RELAP5-3D predicted clad temperatures. After one round of tuning the difference between the predictions of the RELAP-7 model and the RELAP5-3D model was down to a few degrees, about 2.1% difference between the two models (see Table 14). Interestingly, all models predict different jumps in temperature between the core channels, with the tuned RELAP5-3D model predicting the greatest differences in temperature and the RELAP-7 model predicting the smallest differences in temperature as shown in Table 14.

5.2.2 TRANSIENT RESULTS

We also performed a simple transient analysis by changing the power level in a step-wise fashion as shown in Figure 36 and evaluated the temporal profile of the average temperature for each three core-channels. Such temporal profiles are shown in Figure 37 and Figure 38 for RELAP-7 and RELAP5-3D respectively.

From Figure 37 and Figure 38, it is possible to note that the transient simulated by the two codes are very similar. Also note that different in temperature between the three core channels among the two codes still is below 3%.

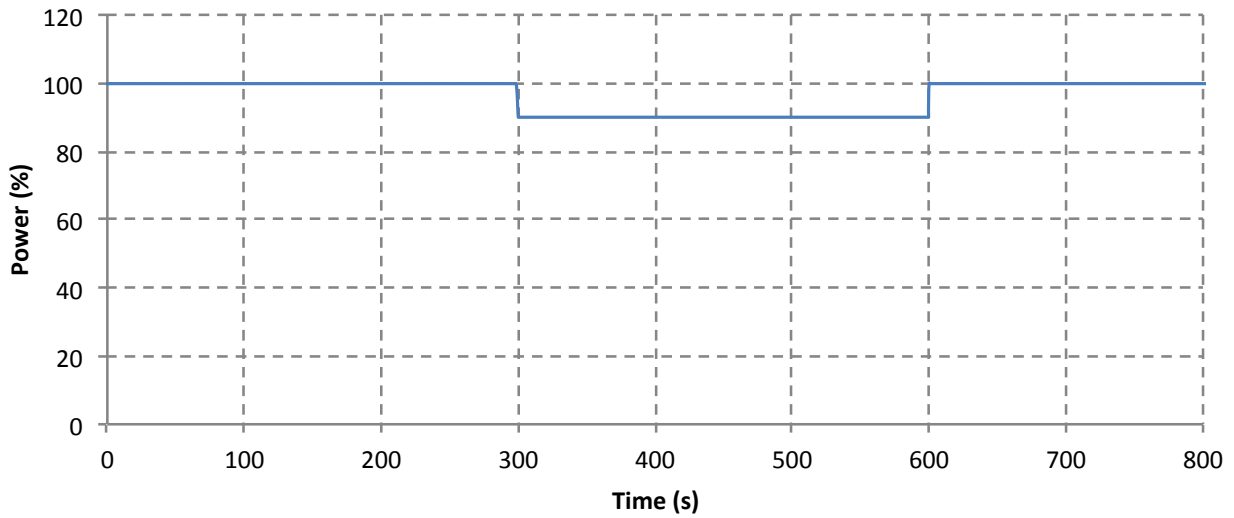


Figure 36: Power transient considered

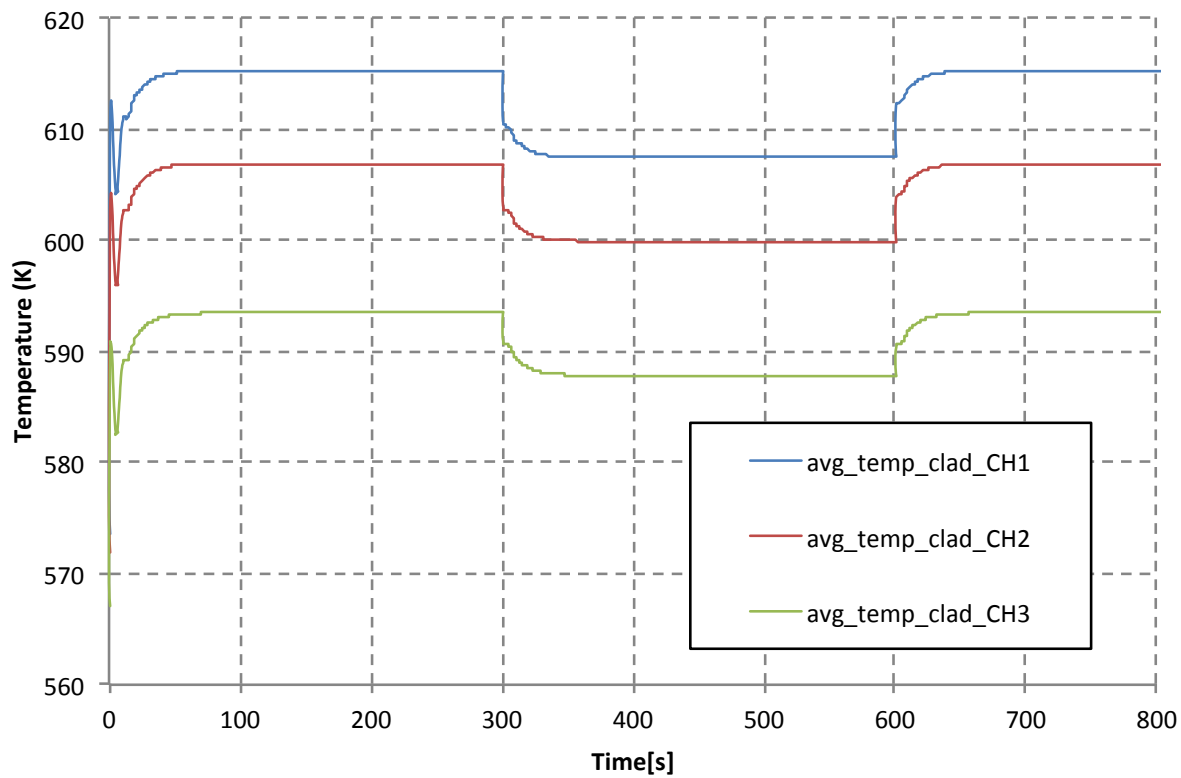


Figure 37: RELAP-7 transient results

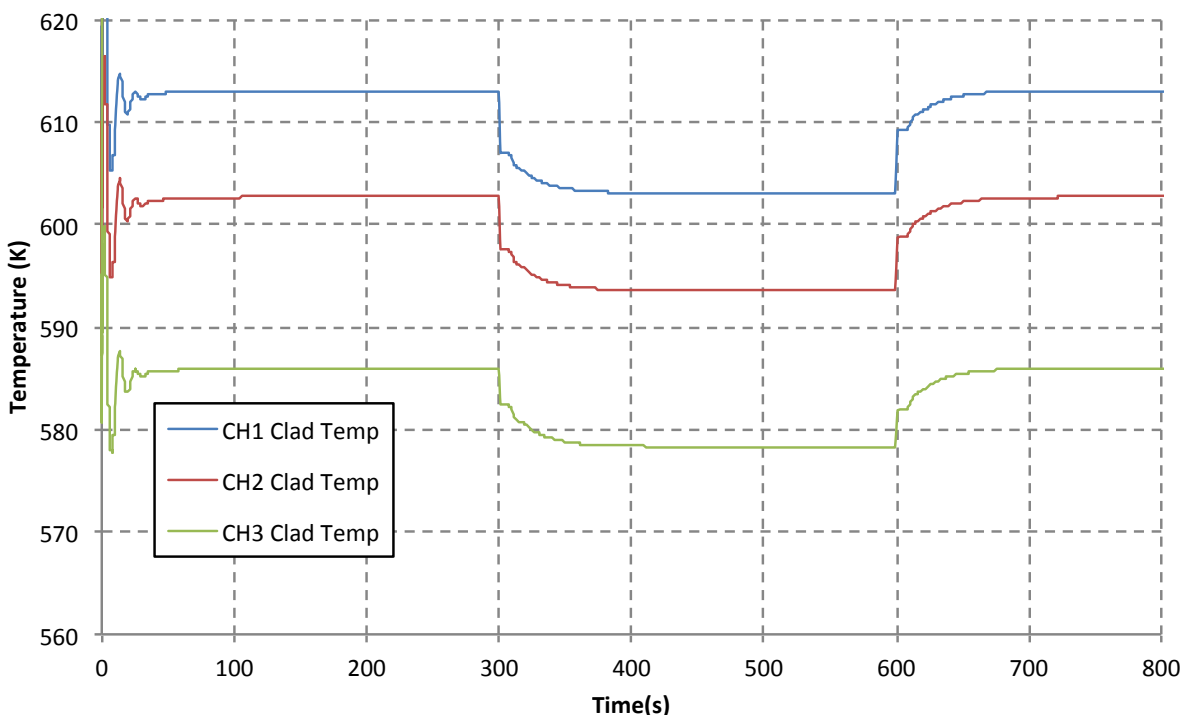


Figure 38: RELAP5-3D transient results

6. RISM TOOLKIT ENHANCEMENTS

Quick and effective accident management is essential in any industry in order to limit and contain possible threats to both people and environment/assets. This ability is in particular relevant in the nuclear industry where accidents may have impacts from an economic, health and societal point of view. As an example, the Fukushima Daiichi and Daini nuclear power plant accidents highlighted the importance of the ability of plant operators and plant staff to react quickly and effectively in accident conditions. This particular event showed the importance of being able to:

- Determine/estimate the actual status of the plant (*diagnosis*) when the monitoring system is corrupted or partially unavailable, and,
- Forecast its future evolution (*prognosis*).

This section describes a research direction geared toward the development of a new set of advanced diagnosis and prognosis tools. We employ innovative data mining and machine learning techniques that are able to infer plant status and mimic the plant's full temporal behavior in order to assist the reactor operators during an accident scenario.

6.1 DIAGNOSIS AND PROGNOSIS: STATE OF PRACTICE AND STATE OF THE ART

Current state-of-practice diagnosis/prognosis tools are the so-called risk-monitors which are mainly based on ET-FT logic structures [24] (see also Section 4.2). The basic idea of this kind of algorithms is that they try to match the actual status of the plant with one or more branches from the ET.

An example is given in Figure 39 for a simplified ET structure for a loss of off-site power (LOOP) scenario. Three events are considered: emergency AC power available (i.e., DGs), AC recovery and FW recovery. System success is guaranteed if any of these three events occurs. The ET shown in Figure 39 can be used to inform the reactor operators about the actual CD probability given the status of the plant when a LOOP event occurs. The risk-monitor continuously monitors the status of specific components/systems of the plant that are also present in the ET structure (e.g., status of the DGs) and associates such status to a specific ET branch or set of ET branches.

Given a hypothetical LOOP transient in a NPP (see Figure 40 top), the following events happen in this sequence: DGs fail to run and AC power cannot be recovered (both DGS and off site power grid switchyard are permanently disabled). The risk-monitor follows this sequence of events that are actually happening in the NPP (see Figure 40 top) and find the appropriate path in the ET (see red branch in Figure 39) that match the plant status.

In addition, the risk-monitor provides information regarding the probability to reach CD (P_{CD}) given the actual status of the plant. Such value of P_{CD} is then updated every time the plant configuration changes (see Figure 40 bottom) from the ET branch or the set of ET branches that matches the plant status.

The output of the risk monitors is not only limited to P_{CD} but it can also rank all the basic events of the FTs associated with each ET branch segment. This ranking can be performed by using several metrics (Birnbaum, Fussell-Vesely or risk reduction worth [41]). This ranking can help the reactor operators to actually focus their attention on the highest ranked components (such as perform additional monitoring) and/or prioritize recovery procedures.

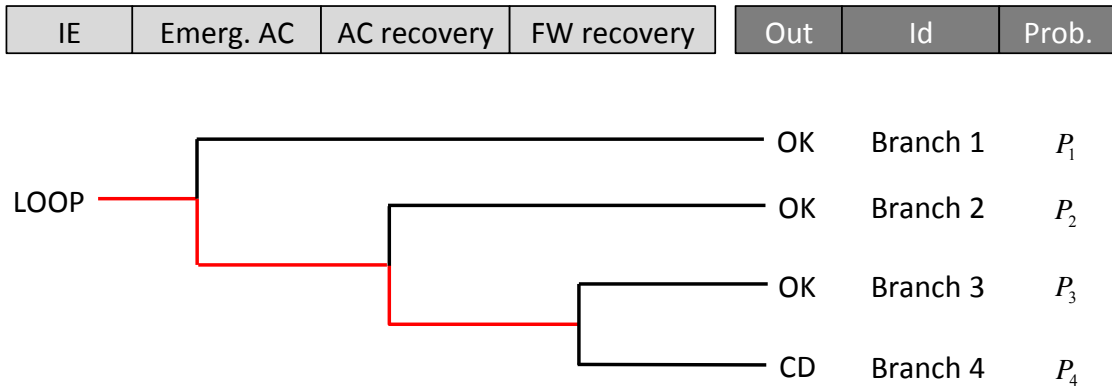


Figure 39: Hypothetical ET structure for a LOOP initiating event

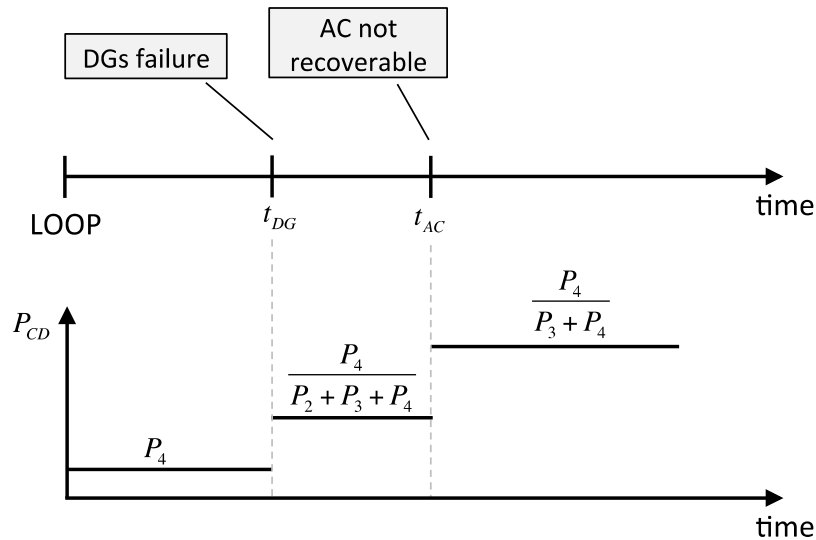


Figure 40: Core Damage probability (P_{CD}) value displayed by an hypothetical ET-FT based risk monitor (bottom) for a LOOP accident scenario (top) using the ET structure shown in Figure 39. The accident scenario is continuously matched with the ET structure. Such match for the accident scenario considered (top) is shown as a red line in Figure 39

One of the major drawbacks of ET based risk-monitors is that they do not actually take into account timing and sequencing of events, i.e., they are “static” risk monitors [24]. Thus, during an accident scenario, only limited amounts of information can be provided to the reactor operators. Such information does not contain any insights regarding actual prediction of system behavior but is limited to providing the probability that a certain outcome (e.g., core damage CD) will occur. In addition, diagnosis capabilities are also limited since status of the plant, in terms of temperature/pressure and level values within the RPV, is not an integral part of the ET/FT structures.

Only lately, research efforts are considering the large amount of data generated by safety analysis codes (e.g., generated by Dynamic PRA methodologies [25]) instead of ET/FT structures to assist reactor operators [26]. The basic idea is to generate a large database of simulated scenarios (for example using

RELAP) where timing and ordering of events are randomly changed. Once this database is created, the risk monitor try to match the status of the plant (in terms of system state variables such as temperature or pressure of specific point of the RPV) with one or more simulated scenarios that have a similar temporal behavior. If the database does not contain enough information to find this match, a series of new simulations are run. These simulations are initialized so that initial conditions of the simulation itself match as close as possible the status of the plant at the beginning of the transient. Once the match between simulated data and plant status is available, the reactor operators can infer the future evolution of the system by looking at the simulated scenarios that match the past history of the transient.

These efforts employ basic data mining techniques in order to estimate the plant status. In addition, they still rely on safety analysis codes to predict system evolution. This may limit their applicability since computational speed for safety analysis codes is fairly low and numerous runs are required to perform such predictions.

6.2 MERGING DATA MINING AND MACHINE LEARNING

Our research direction within the RISMC Pathway aims to extend RISMC capabilities by using advanced data mining and machine learning techniques to move from an *off-line* tool (i.e., safety analysis type of applications) to *on-line* tool (i.e., accident management).

We build “dynamic” approaches that gather data from safety analysis simulation data and historic plant data in order to build surrogate models [12]. These surrogate models are used to infer the actual status of the plant when limited information is available and to predict full temporal behaviors in a very short amount of time (see Figure 41).

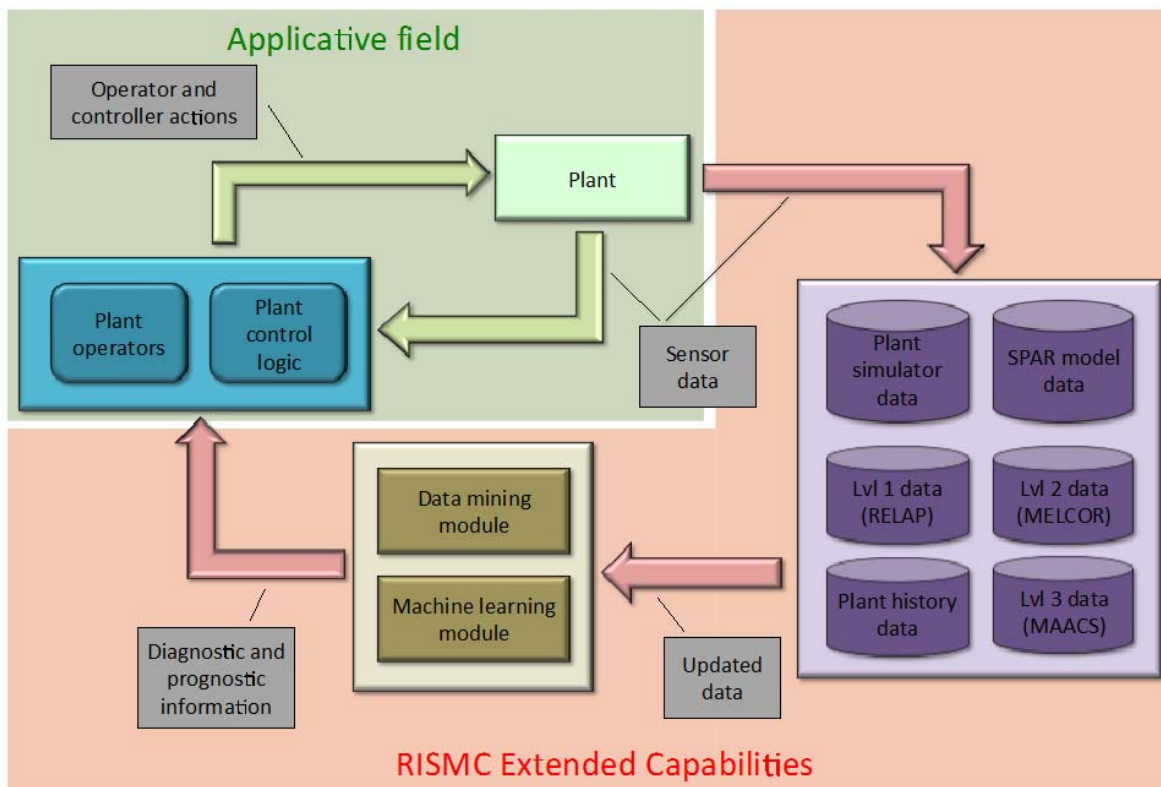


Figure 41: RISMC diagnosis/prognosis framework

These dynamic approaches use advanced data mining techniques to analyze data generated by multiple safety analysis codes, plant history and plant simulators. The analysis of such heterogeneous data sets allow us to create “temporal” reduced order models (ROM), i.e., surrogate models, using machine learning algorithms. These temporal ROMs emulate the full plant dynamics but with much smaller computational time compared to safety analysis codes.

Note that these models can be used for accident management to assist reactor operators during accident scenarios in order to prioritize recovery actions, optimize plant staff resources, and chose optimal recovery paths. These models can also be used to perform: plant data reconstruction and filtering, plant data anomaly detection, reactor operator training, and design of Severe Accident Management Guidelines (SAMGs).

6.3 BASIC MACHINE LEARNING

The main idea behind the concept of a generic reduced order model (ROM) is to reconstruct the function $F(\mathbf{x})$ of a generic system (i.e., a black box) from a finite set of n data points² in a d dimensional space:

$$(\mathbf{x}_i, F(\mathbf{x})_i), \quad i = 1, \dots, n \quad (1)$$

where, for each input parameter:

$$\mathbf{x} \in \mathbb{R}^d, \quad \mathbf{x} = [x_1, \dots, x_d] \quad (2)$$

a system response $F(\mathbf{x}) \in \mathbb{R}$ has been collected.

The reconstruction of $F(\mathbf{x})$, indicated as $\tilde{F}(\mathbf{x})$, is typically performed through a combination of regression and interpolation techniques such that (see Figure 42 for a 1-D case and Figure 43 for a 2-D case)

$$\tilde{F}(\mathbf{x})_i \cong F(\mathbf{x})_i \quad \text{for } i = 1, \dots, n \quad (3)$$

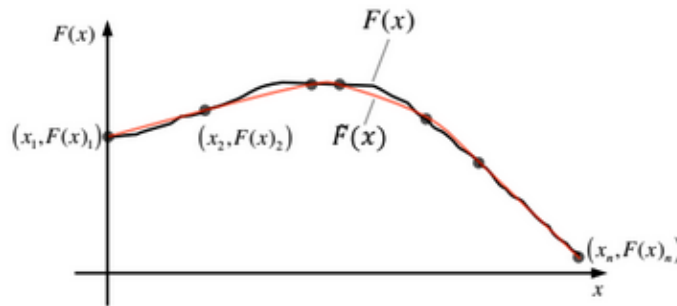


Figure 42: Example of 1-dimensional response surface

² - Points that have been generated either through a measuring or a simulation process.

The reconstructed $\tilde{F}(\mathbf{x})$ is typically known as a surrogate model (SM) or response surface for $F(\mathbf{x})$. Such functions can be generated using a wide variety of algorithms such as: Gaussian Process Models (GPM) [27], Support Vector Machines (SVM) [28, 29], KNN [30] or be based on classical interpolator methods [31].

For simulation-based safety applications, we aim to understand how a safety related parameter (e.g., maximum clad temperature) is affected by the timing and sequencing of events (e.g., recovery of AC power) or the uncertainties associated with characteristic parameters of the simulation. As an example, $\tilde{F}(\mathbf{x})$ are used to reduce the number of samples in a Monte-Carlo analysis through adaptive sampling [29, 32]. In this case, the scope is to determine the system failure probability by randomly sampling \mathbf{x} and simulating system behavior (e.g., maximum clad temperature). Failure probability p_F is calculated as the ratio of the number of simulations that lead to failure over the total number of simulations performed. Since p_F might be very small, a large number of computationally-expensive simulations may be required. Adaptive sampling infers, from a set of training simulations, regions that lead to failure (maximum clad temperature greater than failing temperature) and concentrates samples on those regions.

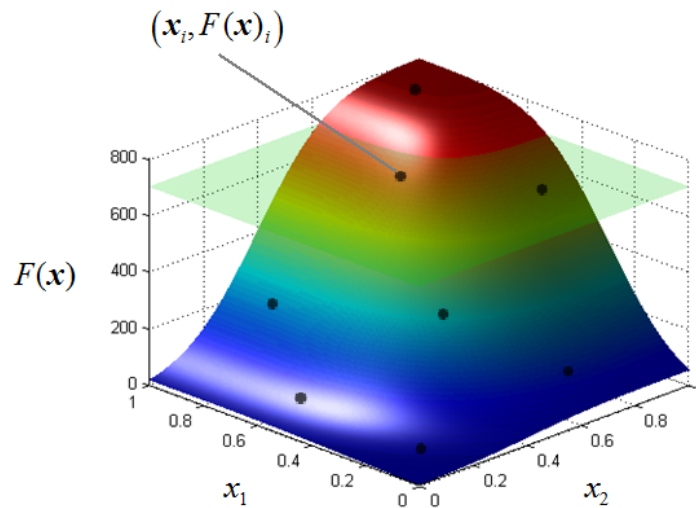


Figure 43: Example of a 2-dimensional response surface

Note that the evaluation of $\tilde{F}(\mathbf{x})$ for a new $\mathbf{x} \neq \mathbf{x}_i$ ($i = 1, \dots, n$) is much less computationally intensive than simulating the exact value $F(\mathbf{x})$. This is in particular true when the evaluation of $F(\mathbf{x})$ can take hours or days. Prediction capabilities lie within the ability to determine system outcomes (e.g., max clad temperature) in a much faster way than real-time.

6.4 TEMPORAL PREDICTOR

In the previous section we introduced the concept of response surface methods and ROMs as tools to predict an approximated $\tilde{F}(\mathbf{x})$ (which represents, for example, a simulated system response under an accident scenario) for a set of conditions specified in \mathbf{x} . The vector \mathbf{x} contains elements x_d such as timing and sequencing of events (e.g., recovery time of AC power, failure time of core cooling injection). Note that the value $\tilde{F}(\mathbf{x})$ is a scalar and, thus, does not contain any temporal evolution type of information.

We extend the concept of ROM in order to be able to handle time dependent $\tilde{F}(\mathbf{x})$: given \mathbf{x} , $\tilde{F}(\mathbf{x}, t)$ is a time dependent variable. In this case, the training consists of n points:

$$(\mathbf{x}_i, F(\mathbf{x}, t)_i) \quad i = 1, \dots, n \quad (4)$$

Our approach is to start by dividing the temporal scale into intervals (assumed here to be of equal length but it is not required):

$$t = [t_1, \dots, t_T] \quad (5)$$

For each time point t_k ($k = 1, \dots, T$) we consider the subset of points:

$$(\mathbf{x}_i, F(\mathbf{x}, t_k)_i) \quad i = 1, \dots, n \quad (6)$$

and we build the corresponding $\tilde{F}(\mathbf{x}_i)_k$. Thus, now we have a set of reduced order models for each time point t_k ($k = 1, \dots, T$). The temporal predictor $\Theta(\mathbf{x}, t)$ is simply the vector of:

$$\Theta(\mathbf{x}, t) = [\tilde{F}(\mathbf{x})_1, \dots, \tilde{F}(\mathbf{x})_k, \dots, \tilde{F}(\mathbf{x})_T] \quad (7)$$

In our applications, when each of the data points has been generated by safety analysis codes (e.g., RELAP, MELCOR [33]):

- \mathbf{x} is the configuration of the simulation (e.g., timing of events, values associated with uncertain parameters)
- $F(\mathbf{x}, t)$ is the simulation associated with \mathbf{x} .

We performed a few tests with different types of datasets in order to identify performances and limitations of this algorithm. Figure 44 shows a set of $n = 20$ simulations, i.e. $F(\mathbf{x}, t)_i$ ($i = 1, \dots, 20$), generated by sampling two stochastic parameters, i.e. $\mathbf{x}_i = [x_1, x_2]$. We initially divided the time scale uniformly $[0, 2500]$ into $T = 100$ intervals and for each time point t_k ($k = 1, \dots, 100$) we considered the data points $(\mathbf{x}_i, F(\mathbf{x}, t_k)_i)$ ($i = 1, \dots, 20$) and built the reduced order models $\tilde{F}(\mathbf{x})_k$. We then tested the temporal predictor $\Theta(\mathbf{x}) = [\tilde{F}(\mathbf{x})_1, \dots, \tilde{F}(\mathbf{x})_{100}]$ for several \mathbf{x}_j ($j \neq i$) and compared them with the simulated $F(\mathbf{x}, t)_j$.

Figure 44 shows the predicted scenario $\Theta(\mathbf{x}, t)$ (green line) and the actual simulated scenario $F(\mathbf{x}, t)$. For this particular case we built $\Theta(\mathbf{x}, t)$ using Gaussian Process Models as basic predictive models. A useful feature is that these algorithms are also capable of providing the uncertainty associated with the predicted results.

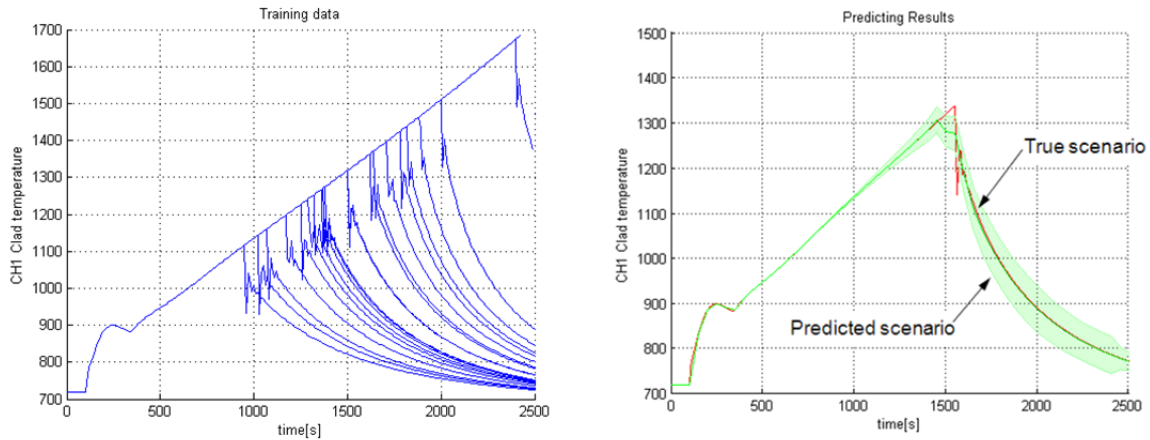


Figure 44: Example of predicted temporal profile (left) given a set of simulated scenarios (right)

6.5 DATA MINING MODULE

While the machine-learning path is predominantly followed within RISMIC for the creation of predictive models, data mining based algorithms can provide useful diagnosis and prognostic capabilities especially for heterogeneous types of data (data generated by different sources or characterized by different types of content information).

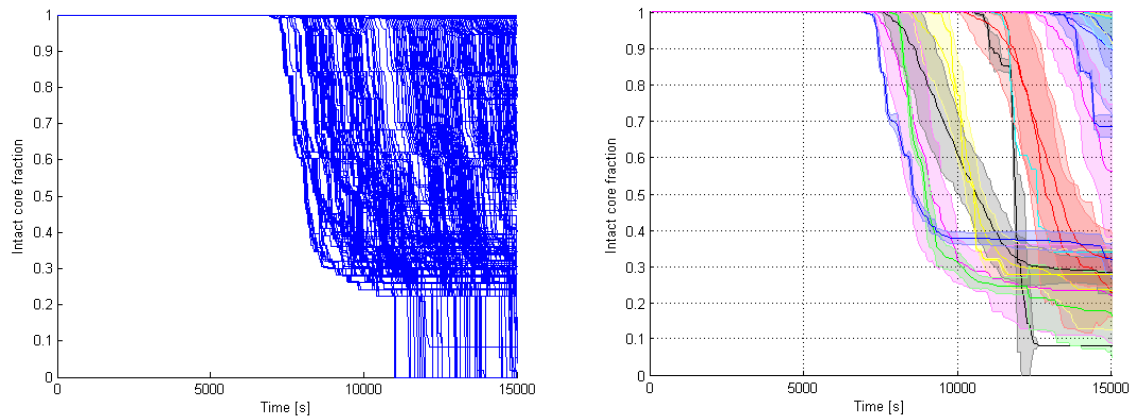


Figure 45: Clustering of simulated scenarios into groups: representative scenarios [34]

As an example, [34] effectively shows how predicting capabilities can be reached using a blend of *clustering* and *dimensionality reduction* techniques.

Starting from a set of simulation runs (e.g., generated by RELAP), dimensionality reduction techniques [35, 36, 37] are used to select the input variables of the simulations that contain larger amounts of information (e.g., temperature or pressure of specific nodes of the simulator). Clustering algorithms [38] are then used to group scenarios that have a similar temporal behavior into clusters and generate, for each

group, a representative scenario [34] (see Figure 45). Each representative scenario is basically an average of the scenario in that particular cluster.

Diagnosis and prognosis capabilities are performed:

1. Querying the actual or the past status of the plant
2. Identifying representative scenario(s) that better match the information coming from 1.

By using the representative scenario(s) found in 2) it is possible to forecast system evolution (prognosis) or identify the system configuration that leads to that particular temporal evolution (diagnosis).

While we believe that such approach is sound, we also think that some limitations may occur for very large quantities of heterogeneous types of data. Most clustering algorithms, in fact, assume the data points are homogenous. We aim to deal with very *heterogeneous* types of data: plant history data, plant simulator data, simulated data (by using safety analysis codes for example) but also data generated by ETs and FTs.

In order to overcome the limitations indicated above for the approach presented in [39] we have identified data *symbolic conversion* as possible solution. Symbolic conversion means data numeric data is converted as a sequence of letters/symbols [40]. Note that data generated by FT-ET based methodologies generate by definition symbolic data where each symbol in a cut set represents the status of a particular component system.

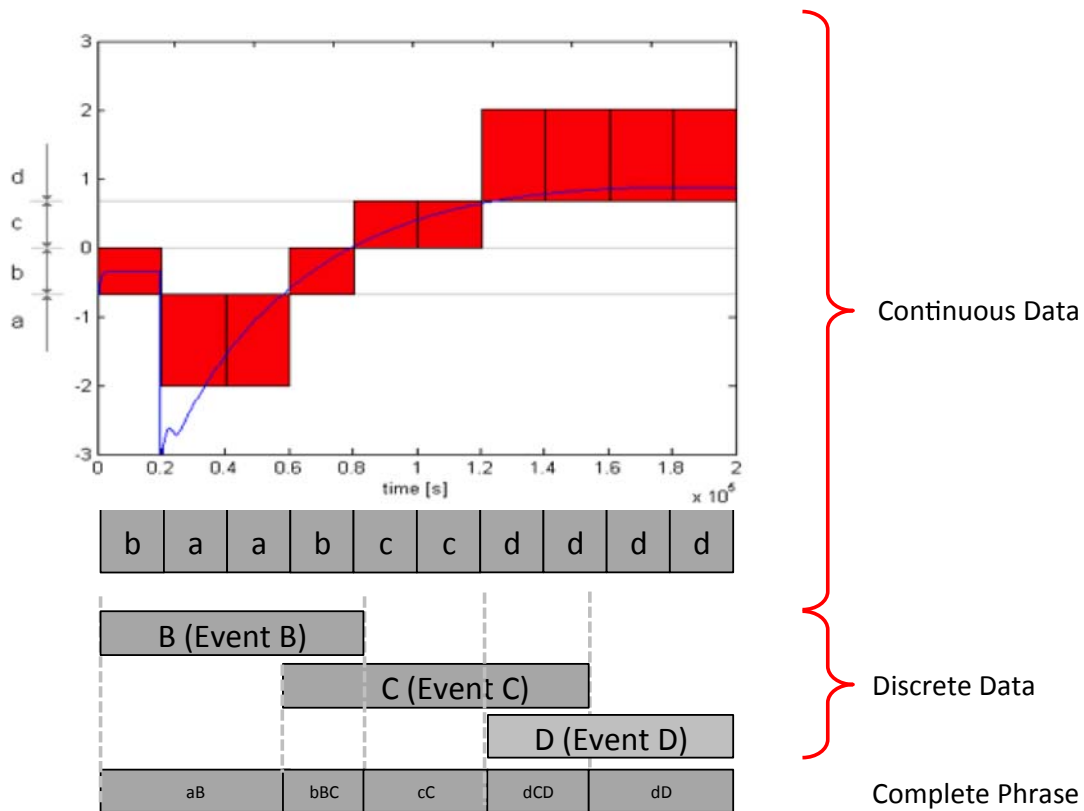


Figure 46: Symbolic conversion of time dependent data [39]

However, data generated by safety analysis codes, simulated in the system simulator or historic data measured directly from the plant contains two types of datasets:

- *Continuous data*: which contains temporal profiles of state variables (e.g., temperature, pressure of specific nodes of the simulator)
- *Discrete data*: which contains timing of events. Note that a generic event can occur at a time instant or over a time interval.

As shown in Figure 46 (and without going into details), symbolic conversion is accomplished by [39]:

1. Quantizing both datasets separately
2. Associating to each quantized element a symbol
3. Merging the two symbolic sentences accordingly to their temporal order

The advantages of using symbolic data are indicated in (see Table 15):

- Efficiencies in data storage reduction
- Faster clustering/classification computation
- Availability of tools such as Markov Models, Decision Trees or Hashing algorithms.

Table 15: Computational time of search algorithm KNN for three different data set for both real-valued (original) and symbolic data

Dataset	Size	Avg. time (real-valued)	Avg. time (symbolic)
Data 1	7 MB	4.1 ± 0.75 s	0.2 ± 0.03 s
Data 2	362 MB	12 ± 2.1 s	0.95 ± 0.12 s
Data 3	3.2 GB	4.1 ± 0.75 s	0.2 ± 0.03 s

In addition, symbolic conversion can readily fit into diagnosis/prognosis purposes since it allows the user to perform motif discovery, anomaly detection, and sub-series clustering much more easily. In [39], we have shown how such conversion has allowed us to greatly reduce computational time of both searching and clustering algorithms.

7. CONCLUSIONS

In this document we have reported the R&D developments within the RISMIC pathway for the Fiscal Year 2014. We followed three different parallel directions which allow us to:

1. Compare the RISMIC approach with state-of-practice tools (i.e., ET-FT based)
2. Show RISMIC approach capabilities as decision-making tool for a power uprate case
3. Present an extension of the RISMIC approach as reactor operator aiding tool.

In (1) we showed that a simulation based PRA analysis for a BWR SBO accident scenario generated a core damage probability value similar to the one calculated using an ET-FT methodology using SAPHIRE. At this point the following may arise from the reader:

Are the efforts³ required by the RISMIC approach worth the results that can be obtained using state-of-practice methodologies?

From our perspective we believe that simulation based methods are the natural extension traditional methods. An extension that aims to overcome the natural limitations of the latter ones such as: user-defined accident progression and lack system dynamic feedback into timing/sequencing of events. So now, the question presented above is replied by the following:

Are these two limitations justifiable to employ classical tools (ET-FT) for the applications targeted by the RISMIC pathway?

We believe that the answer for such question is negative. Neither power uprate nor ageing are implicitly taken into account in an ET-FT based methodology. They could only be considered in the actual approximated computation of the ET branches or FT basic event probabilities without modeling their actual feedback on timing/sequencing of events.

This has been proven in (2) where we employed the RISMIC approach to evaluate impact, from a statistical point of view, of power uprate for a BWR SBO accident scenario. The actual power uprate was implicitly modeled in the RELAP5-3D simulator while the distributions of the uncertain parameters remained unchanged. In an ET-FT approach, a power uprate would have required a “re-computation” of the FT basic events and/or the ET branching probabilities. Such computation would involve few system simulator runs in order to assess the time needed for certain basic events to occur before CD status is reached. In the RISMIC approach such computation is implicitly embedded in the sampling process of the simulation run internal parameters. In addition, it is worth noticing that by using the RISMIC approach, a much larger amount of information is actually generated. In this report we have shown several limit surfaces which have the capability to visualize how the failure region expands in the input space due to the power uprate.

In (3) we have shown how the RISMIC capabilities can be conceptually employed not only as a PRA tool but also as risk monitor tool to help the user to assess the status of the plant (diagnosis) and predict future evolution of the system during an accident scenario (prognosis). This approach is often identified as risk monitor but we believed such definition might be too limited since a) risk monitors are not designed to be diagnosis tools and b) their predictions do not consider actual possible system accident evolutions.

³ - The efforts considered here are grouped in two classes:

- Modeling: efforts needed to build a validated and reliable system simulator
- Computational: efforts needed to run many (order of thousands) simulation runs and need for high performance computing (HPC) resources

REFERENCES

- [1] C. Smith, C. Rabiti, and R. Martineau, “Risk Informed Safety Margins Characterization (RISMC) pathway technical program plan”, Idaho National Laboratory Technical Report INL/EXT-11-22977 (2011).
- [2] D. Mandelli, C. Smith, S. Prescott, A. Alfonsi, C. Rabiti, J. Cogliati and R. Kinoshita, “Analysis of PWR SBO caused by external flooding using the RISMC toolkit,” Idaho National Laboratory Technical Report INL/EXT-14-32907 (2013).
- [3] U.S. NRC, NUREG 1150, “Severe accident risks: an assessment for five U.S. nuclear power plants,” Division of Systems Research, Office of Nuclear Regulatory Research, U.S. Nuclear Regulatory Commission, Washington, DC (1990).
- [4] RELAP5 Code Development Team, “RELAP5-3D Code Manual”, Idaho National Laboratory Technical Report INEEL-EXT-98-00834 (2012).
- [5] A. David, R. Berry, D. Gaston, R. Martineau, J. Peterson, H. Zhang, H. Zhao, L. Zou, “RELAP-7 Level 2 milestone report: demonstration of a steady state single phase PWR simulation with RELAP-7,” Idaho National Laboratory Technical Report INL/EXT-12-25924 (2012).
- [6] C. Rabiti, D. Mandelli, A. Alfonsi, J. Cogliati, and B. Kinoshita, “Mathematical framework for the analysis of dynamic stochastic systems with the raven code,” in *Proceedings of International Conference of mathematics and Computational Methods Applied to Nuclear Science and Engineering (M&C 2013)*, Sun Valley (Idaho) (2013).
- [7] A. Alfonsi, C. Rabiti, D. Mandelli, J. Cogliati, and R. Kinoshita, “Raven as a tool for dynamic probabilistic risk assessment: Software overview,” in *Proceedings of International Conference of mathematics and Computational Methods Applied to Nuclear Science and Engineering (M&C 2013)*, Sun Valley (Idaho), (2013).
- [8] C. Rabiti, A. Alfonsi, D. Mandelli, J. Cogliati, R. Martinueau, C. Smith, “Deployment and overview of RAVEN capabilities for a probabilistic risk assessment demo for a PWR Station blackout,” Idaho National Laboratory Technical Report INL/EXT-13-29510 (2013).
- [9] E. Zio, M. Marseguerra, J. Devooight, and P. Labeau, “A concept paper on dynamic reliability via Monte Carlo simulation,” in *Mathematics and Computers in Simulation*, **47**, pp. 371-382, (1998).
- [10] J.C. Helton and F. J. Davis, “Latin hypercube sampling and the propagation of uncertainty in analyses of complex systems,” *Reliability Engineering & System Safety*, **81**-1 (2003).
- [11] A. Amendola and G. Reina, “Dylam-1, a software package for event sequence and consequence spectrum methodology,” in EUR-924, CEC-JRC. ISPRA: Commission of the European Communities (1984).
- [12] N.V. Queipo, R.T. Haftka, W. Shyy, T. Goel, R. Vaidyanathan, P.K. Tucker, “Surrogate-based analysis and optimization,” *Progress in Aerospace Sciences*, **41**, pp. 1-28 (2005).
- [13] C. Rabiti, A. Alfonsi, D. Mandelli, J. Cogliati, R. Martinueau, C. Smith, “Deployment and Overview of RAVEN Capabilities for a Probabilistic Risk Assessment Demo for a PWR Station Blackout,” Idaho National Laboratory Technical Report INL/EXT-13-29510 (2013).

- [14] C. Rabiti, A. Alfonsi, D. Mandelli, J. Cogliati and R. Kinoshita, “Advanced probabilistic risk analysis using RAVEN and RELAP-7”, Idaho National Laboratory Technical Report INL/EXT-14-32491 (2014).
- [15] A. Alfonsi, C. Rabiti, D. Mandelli, J. Cogliati, and R. Kinoshita, “RAVEN: Dynamic event tree approach,” Idaho National Laboratory Technical Report INL/EXT-13-30203 (2013).
- [16] D. Mandelli, C. Smith, T. Riley, J. Schroeder, C. Rabiti, A. Alfonsi, J. Nielsen, D. Maljovec, B. Wang, and V. Pascucci, “Support and modeling for the boiling water reactor station black out case study using RELAP and RAVEN,” Idaho National Laboratory Technical Report INL/EXT-13-30203 (2013).
- [17] S. Eide et al, “Reevaluation of station blackout risk at nuclear power plants”, U. S. Nuclear Regulatory Commission, NUREG/CR-6890 Vol. 1, Analysis of Loss of Offsite Power Events: 1986-2004 (2005).
- [18] S. Eide et al, “Reevaluation of station blackout risk at nuclear power plants”, U. S. Nuclear Regulatory Commission, NUREG/CR-6890 Vol. 2, Analysis of Station Blackout Risk (2005).
- [19] R. Sherry and J. Gabor, “Pilot Application of Risk Informed Safety Margins to Support Nuclear Plant Long Term Operation Decisions – Impacts on Safety Margins of Power Uprates for Loss of Main Feed-water Events”, EPRI, Palo Alto, CA, 1025291 (2012).
- [20] U.S.NRC, “NUREG/CR-7110 State-of-the-Art Reactor Consequence Analysis (SOARCA) Project Surry Integrate Analyses Report” Volume IV.
- [21] D. Gertman, H. Blackman, J. Marble, J. Byers and C. Smith, “NUREG/CR-6883: The SPAR-H Human Reliability Analysis Method”, Nuclear Regulatory Commission US-NRC (2005).
- [22] Institute of Nuclear Power Operations, “Special Report on the nuclear accident at the Fukushima Daiichi nuclear power station”, INPO report 11-005 (2011).
- [23] Z. Ma, J. Schroeder, “Event Tree Success Branch Modeling Approaches in SAPHIRE/SPAR,” *Transaction of the American Nuclear Society*, **110**, pp. 349-351 (2014).
- [24] International Atomic Energy Agency (IAEA), “Risk management: A tool for improving nuclear power plant performance”, IAEA-TECDOC-1209 (2001).
- [25] N. Siu, “Risk assessment for dynamic systems: an overview,” *Reliability Engineering and System Safety*, **43**, no. 1, pp. 43-73 (1994).
- [26] K. A. Makinson, “Preliminary framework for the run-ahead predictive simulation software (RAPSS)”, Ph.D. dissertation, Oregon State University (2013).
- [27] C. E. Rasmussen, “Gaussian Processes in machine learning,” *Advanced Lectures on Machine Learning. Lecture Notes in Computer Science* **3176**, pp. 63-71 (2004).
- [28] C. J. C. Burges, “A tutorial on Support Vector Machines for pattern recognition,” *Data Min. Knowl. Discov.* **2-2**, pp. 121-167 (1998).

- [29] D. Mandelli and C. Smith, "Adaptive sampling using support vector machines," in *Proceeding of American Nuclear Society (ANS)*, San Diego (CA), **107**, pp. 736-738 (2012).
- [30] N. S. Altman, "An introduction to kernel and nearest-neighbor nonparametric regression", *The American Statistician*, **46-3**: 175-185 (1992).
- [31] C. Habermann, F. Kindermann, "Multidimensional spline interpolation: theory and applications", *Computational Economics*, **30-2**, pp. 153-169 (2007).
- [32] D. Maljovec, B. Wang, V. Pascucci, P.-T. Bremer, and D. Mandelli, "Adaptive sampling algorithms for probabilistic risk assessment of nuclear simulations," in ANS PSA 2013 International Topical Meeting on Probabilistic Safety Assessment and Analysis Columbia, SC, on CD-ROM, American Nuclear Society, LaGrange Park, IL (2013).
- [33] R. O. Gauntt, MELCOR Computer Code Manual, Version 1.8.5, Vol. 2, Rev. 2. Sandia National Laboratories, NUREG/CR-6119.
- [34] D. Mandelli, A. Yilmaz, T. Aldemir, K. Metzroth, and R. Denning, "Scenario clustering and dynamic probabilistic risk assessment," *Reliability Engineering & System Safety* **115**, pp. 146-160 (2013).
- [35] J. B. Tenenbaum, V. de Silva, and J. C. Langford, "A global geometric framework for nonlinear dimensionality reduction," *Science*, **290**, pp. 2319-2323 (2000).
- [36] D. Mandelli, A. Yilmaz, and T. Aldemir, "Clustering on manifolds: an application to scenario analysis using principal component analysis," in *Proceeding of American Nuclear Society (ANS)*, Washington (DC) (2011).
- [37] D. Mandelli, A. Yilmaz, and T. Aldemir, "Clustering scenarios on manifolds," in *Proceeding of American Nuclear Society (ANS)* (2011).
- [38] A. K. Jain, K. Dubes, and C. Richard, *Algorithms for clustering data*, Upper Saddle River, NJ (USA): Prentice-Hall, Inc. (1988).
- [39] D. Mandelli, C. Smith, A. Yilmaz, and T. Aldemir, "Mining nuclear transient data through symbolic conversion," in *ANS PSA 2013 International Topical Meeting on Probabilistic Safety Assessment and Analysis*, Columbia, SC, on CD-ROM, American Nuclear Society, LaGrange Park, IL (2013).
- [40] J. Lin, E. Keogh, S. Lonardi and B. Chiu, "A symbolic representation of time series, with implications for streaming algorithms", In *Proceedings of the 8th ACM SIGMOD Workshop on Research Issues in Data Mining and Knowledge Discovery*, San Diego (2003).
- [41] M. van der Borst, H. Schoonakker, "An overview of PSA importance measures," *Reliability Engineering and System Safety*, **72-3**, pp. 241-245(5) (2001).

APPENDIX A: LIMIT SURFACE EVALUATION

In this section it is explained how the limit surfaces shown in Section 3.5 have been evaluated. We employed Support Vector Machine (SVM) based algorithms [28,29].

Given a set of N multi-dimensional samples \mathbf{x}_i and their associated results $y_i = \pm 1$ (e.g., $y_i = +1$ for system success and $y_i = -1$ for system failure), the SVM finds the boundary (i.e., the decision function) that separates the set of points having different y_i . The decision function lies between the support hyper-planes which are required to:

- Pass through at least one sample of each class (called support vectors)
- Not contain samples within them

For the linear case, see Figure A-1, the decision function is chosen such that distance between the support hyper-planes is maximized.

Without going into the mathematical details, the determination of the hyper-planes is performed recursively and updated every time a new sample has been generated. Figure A-1 shows the SVM decision function and the hyper-planes for a set of points in a 2-dimensional space having two different outcomes: $y_i = +1$ (green) and $y_i = -1$ (red).

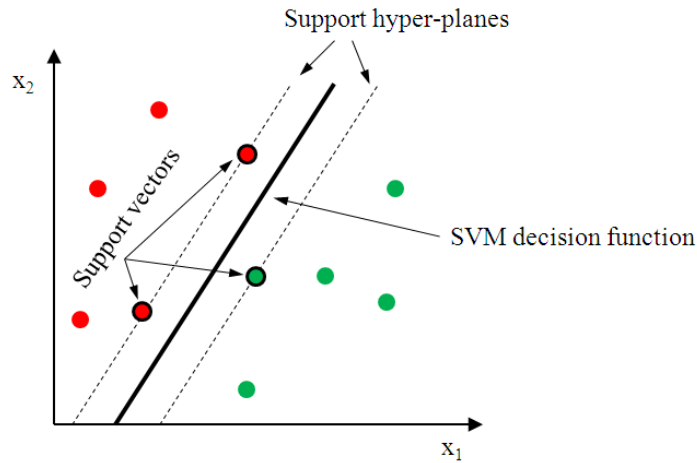


Figure A-1: Limit surface evaluation using SVMs

The transition from a linear to a generic non-linear hyper-plane is performed using the kernel trick. This process involves the projection of the original samples into a higher dimensional space known as featured space generated by kernel functions $K(\mathbf{x}_i, \mathbf{x}_j)$:

$$K(\mathbf{x}_i, \mathbf{x}_j) = \exp\left(-\frac{\|\mathbf{x}_i - \mathbf{x}_j\|}{2\sigma^2}\right)$$